Modelling wave attenuation by salt marsh vegetation

A porous layer approach with CoastalFOAM

Wessel den Heijer

University of Twente

UNIVERSITY OF TWENTE.

Modelling wave attenuation by salt marsh vegetation

A porous layer approach with CoastalFOAM

by

Wessel den Heijer

to obtain the degree of Master of Science
at the University of Twente
to be defended publicly on Thursday August 29, 2024 at 2:00 PM.

Chair supervisor (UT):	dr. ir. B.W. (Bas) Borsje
Daily supervisor (UT):	dr. ir. E.M. (Erik) Horstman
Supervisor (RHDHV):	ir. L.P. (Luc) van Koelen
Supervisor (RHDHV):	ir. M.C. (Marc) Horstman
Project Duration:	February 14, 2024 - August 29, 2024

Cover: Salt marsh (Rupprecht, 2015)

UNIVERSITY OF TWENTE.

Royal HaskoningDHV
Enhancing Society Together

Preface

This thesis for my master's degree in civil engineering and management, with a specialization in river and coastal engineering, was conducted in collaboration with the University of Twente and Royal-HaskoningDHV. I have learned a lot during this thesis project and would like to thank everyone involved.

My greatest thanks go to my supervisors: Luc van Koelen, Erik Horstman, Marc Horstman and Bas Borsje. Luc van Koelen, your expertise in the field of wave modeling and way of providing feedback has helped me to understand the research. Your open-door policy and involvement in social activities at RoyalHaskoningDHV have provided me with a welcoming and enriching environment. Erik Horstman played a crucial role in maintaining the academic level of this thesis, providing both critical feedback and support. Marc Horstman played a crucial role in starting up the project and the model.

In addition to my supervisors, I would like to express my gratitude to Maike Paul, who provided the data necessary for my research.

Lastly, I want to thank my family and friends for their support during this journey and everyone else who contributed to this thesis project.

I hope you enjoy reading this thesis.

Wessel den Heijer
Rotterdam, August 2024

Abstract

Salt marshes known for their wave attenuation capabilities have garnered attention because they can protect low-lying areas sustainably from larger and more powerful waves resulting from extreme weather events. CoastalFOAM is a computational fluid dynamics model (CFD), which is able to simulate sea waves in a numerical wave flume. The model's capability to accurately compute wave overtopping and wave loads enables the assessment of salt marsh vegetation in front of dikes as a strategy to reduce these failure mechanisms, potentially leading to lower design requirements for the dikes. However, CoastalFOAM is a 2D vertical model, posing challenges when modelling wave attenuation using the conventional 3D cylinder method. Nevertheless, the model can simulate flow velocity reduction in a stone layer by representing it as a porous layer. This leads to the research question: 'How can a porous layer within CoastalFOAM be effectively used to model wave attenuation during storm conditions by salt marsh vegetation at the foreshore of a dike?'.

The porous layer, representing the damping capacity of salt marsh vegetation, can decrease the orbital velocity of sea waves. The Darcy-Forchheimer equation is used to quantify this damping effect. For stone layers, physical characteristics are defined by median grain size (D_{50}) and porosity (n_p). Assuming a comparable scale for $D50$ and pore size, D_{50} can be equated to the distance between grass stems. Porosity is considered the ratio of total volume from the ground to stem height to the same volume excluding stems. Although the physical parameters can now be determined, the Darcy-Forchheimer equation includes two calibration parameters: α, β. The values of α and β determine the relative importance of laminar and turbulent flow within the equation. This importance is assessed using the porous Reynolds number (Re_p).

A flume study on wave attenuation by a salt marsh is used to calibrate the model and run sensitivity tests. Three tests are selected: the base case, a tests with a higher wave and a test with lower vegetation height. The value of (Re_p) is higher than 300 for the tests, which indicates that α is negligible, leaving only β to be calibrated. With all parameters of the Darcy-Forchheimer equation known, the calibration of β remains. The optimal value for β equals 4.84 for the base case.

The model accurately replicates significant wave height reduction, peak wave period changes, and wave spectra for the base case, demonstrating agreement with the physical flume experiment. However, when simulating higher waves in the second test, the model overestimated wave height reduction, showing a reduction of 23.6% instead of the observed 13.9% reduction. This difference could be attributed to the model's assumption of rigid grass stems, as real-world grass demonstrates bending. To address this, deriving a relationship between the calibration parameter β and stem bending could improve model applicability. The mowed vegetation test, with a height less than 10% of the original vegetation height, underestimated wave reduction, showing a reduction of 2.5% instead of the observed 7.5% reduction. This difference might come from either the incorporation of bottom friction within the porous layer or the model's inability to accurately capture plant bending. Decoupling bottom friction and the porous layer, potentially using a gradient boundary condition or two separate porous layers, could resolve the bottom friction issue.

Although the model accurately represents wave attenuation for the base case, it currently faces limitations in accounting for variations in hydrodynamic conditions or vegetation characteristics without recalibration. This method can be extended to mangroves or willow forests, which align better with the rigid stem assumption. However, factors such as vertical layers, uniform stem distribution, and emergent vegetation instead of submerged can introduce additional complexities.

List of Figures

List of Tables

Nomenclature

Abbreviations

Abbreviation	Definition
CFD	Computational fluid dynamics
RANS	Reynolds-averaged Navier-Stokes
JONSWAP	Joint North Sea Wave Project spectrum
WG	Wave gauge
CFE	CoastalFOAM flume experiment
PFE	Physical flume experiment

Symbols

Symbol	Definition	Unit
a	Darcy term	[-]
b	Forchheimer term	$[s/m]$
C_d	Drag coefficient	[-]
C_m	Mass coefficient	[-]
D_{50}	Median grain size	$[m]$
f	Wave frequency	$[Hz]$
F_p	Resistance force porous layer	$[N/m^3]$
F_x	Vegetation drag	$[N/m^3]$
g	Gravitational acceleration	$[m/s^2]$
h	Water depth	$[m]$
H_i	Individual wave height	[m]
H_{m0}	Zeroth moment wave height	$[m]$
H_{rms}	Root mean square wave height	$[m]$
KC	Keulegan-Carpenter number	[-]
L	Length of the salt marsh	$[m]$
L_f	Length of the numerical wave flume	$[m]$
m_0	Zeroth moment of the wave spectrum	$[m^2]$
N_i	Number of incident waves	[-]
N_p	porosity of porous layer	[-]
p^*	Excess pressure	$[N/m^2]$
Re_p	Porous Reynolds number	[-]
S_d	Stem diameter	$[m]$
S_h	Stem height	$[m]$
S_n	Stem density	$[stems/m^2]$
t	Time	$[s]$
T	Wave period	$[s]$
$T_{m-0.1}$	Spectral wave period	$[s]$
T_p	Peak wave period	$[s]$
u	Orbital velocity	$[m/s]$
u_f	Filter velocity vector in Cartesian coordinates	$[m/s]$
u_m	Maximum oscillating velocity	$[m/s]$
$\overline{u}$	Averaged flow velocity	$[m/s]$
V	Velocity	$[m/s]$

Symbol	Definition	Unit
x	Cartesian coordinate vector (in line with the direction of the propagation of the wave)	[m]
y	Cartesian coordinate vector (perpendicular to the direction of the propagation of the wave)	[m]
z	Cartesian coordinate vector (in the direction of the water column)	[m]
α	Calibration parameter Darcy term	[s/m]
β	Calibration parameter Forchheimer term	[s]
ΔS	Space between stems	[m]
λ	Wave length	[m]
μ_u	Dynamic viscosity	[Ns/m^2]
ν	Kinematic viscosity	[m^2/s]
ρ	Density	[kg/m^3]
ρ_b	Dry bulk density	[kg/m^3]
ρ_s	Soil particles density	[kg/m^3]

Contents

1

Introduction

1.1. State of the art

Extreme weather events are intensifying, leading to larger waves. In addition, sea level rise will increase the pressure on coastal flood protection (Lambers, 2022). As a consequence, many of those living in low-lying areas around the world face a growing threat of flooding (Adesina et al., 2024; De Jesus Crespo et al., 2019; van Wesenbeeck et al., 2022). In a world increasingly focused on sustainability, coastal defense systems are undergoing a transformation. Nature-based solutions are being increasingly used alongside hard structures for shoreline protection, with the goal of minimizing the design requirements for these hard structures and thereby reducing their overall environmental impact. Therefore there is a growing interest in combining the nature-based coastal defense function of tidal wetlands with engineered coastal defense structures such as dikes (Stark et al., 2016).

The vegetated foreshore refers to the area in front of a dike, often characterized as an intertidal zone with vegetation. This area experiences periodic inundation, which results in a water level on the vegetated foreshore, as illustrated in figure 1.1. The waves that occur together with elevated water levels during storms influence critical aspects such as wave overtopping and wave loads on dikes, representing failure mechanisms for the dikes. Vegetated foreshores, such as salt marshes and mangroves, are increasingly recognized globally for their effectiveness in reducing wave heights, which in turn reduces wave overtopping and wave loads on dikes, among other advantages. By adopting this approach, the dike could comply with flood protection requirement goals with a reduced height or width. Although existing dikes will not be reduced in width or height, this approach could potentially avoid the need for future dike upgrades. Besides along coastlines there is also potential for reducing wave height and run-up in rivers and lakes by floodplain vegetation and riparian forests like willows (van Wesenbeeck et al., 2022).

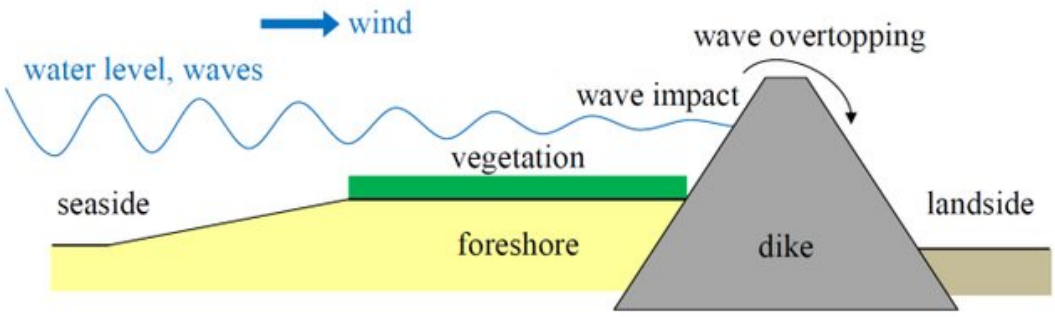

Figure 1.1: Vegetated foreshore in front of a dike (Vuik et al., 2016b)

Figure 1.2 shows that the salt marshes grow all over the world, but the most salt marshes are found in temperate climates such as the Netherlands.

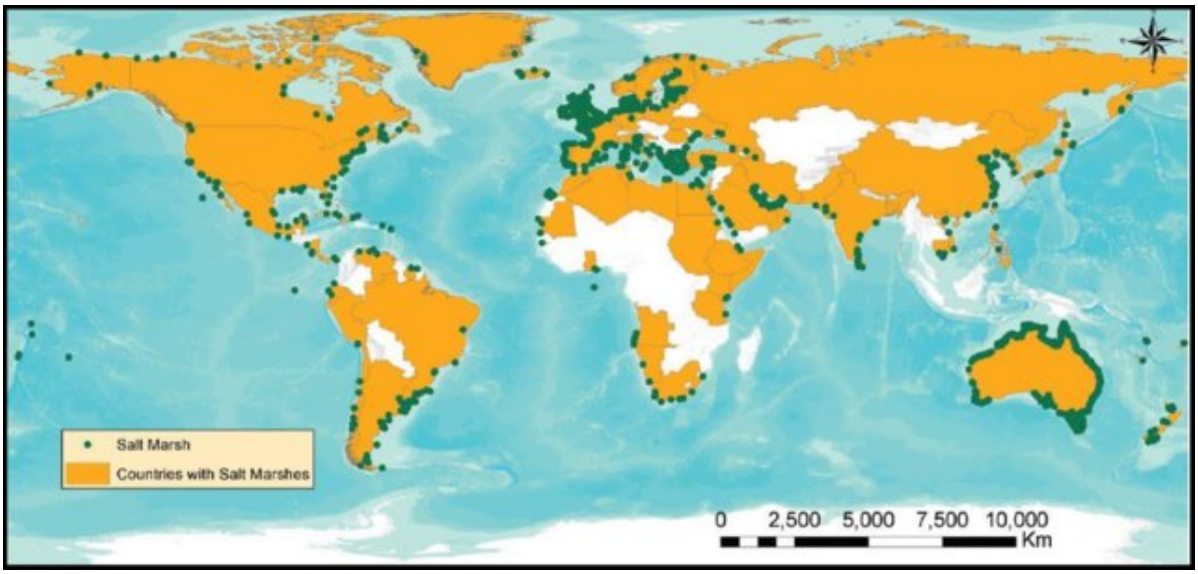

Figure 1.2: Global distribution of salt marshes (O'hara, 2017)

The ability of trees and salt marshes to attenuate waves and mitigate storm damages receives massive attention (van Wesenbeeck et al., 2022). Researchers employ field studies (Haddad et al., 2024; Horstman et al., 2014), laboratory experiments (Çete, 2019; Möller et al., 2014), and numerical models (Phan et al., 2019; Takagi, 2023; Vuik et al., 2016a; Yin et al., 2023a) to understand the mechanisms behind wave attenuation facilitated by vegetation. Field studies provide real-world data on wave-vegetation interaction, while laboratory experiments can isolate specific factors influencing wave attenuation. These findings are used to calibrate numerical models that can predict wave behavior under various conditions and across larger scales.

Numerical models for wave attenuation by vegetation typically rely on the simplified shallow water equations (Maza et al., 2015). This limits their ability to represent complex flow features. The models based on the Reynolds-Averaged Navier-Stokes (RANS) equations are called computational fluid dynamics (CFD) models. These models allow a more accurate simulation of the effect of flow through vegetation, including vertical motion, interactions between water and air, and turbulence effects. Water-air interaction plays a crucial role in wave breaking, where waves encounter shallower water and ultimately break. It also affects wave overtopping, the splashing of water over coastal structures, and wave loads, the forces exerted by waves on these structures (Maza et al., 2015; Paulsen et al., 2014).

OpenFOAM models like IHFOAM (Wang et al., 2020) and CoastalFOAM (Boersen et al., 2019) are CFD models. CoastalFOAM, a numerical wave flume model developed by RoyalHaskoningDHV and others, has demonstrated its advantages in predicting wave loads (Jacobsen et al., 2018) and wave overtopping (Boersen et al., 2019) compared to other methods like design rules. This improved accuracy of CoastalFOAM in predicting dike failure mechanisms can be extended by incorporating the effect of a vegetated foreshore on wave attenuation, allowing for more accurate predictions of failure mechanisms and therefore an improvement of dike design criteria.

1.2. Problem description

Section 1.1 reveals the benefit of incorporating wave attenuation by vegetation into CoastalFOAM. Currently, CoastalFOAM lacks the capability to simulate this phenomenon. The standard method of modeling vegetation utilizes cylinders with a drag coefficient. However, CoastalFOAM is a 2D-vertical model,

therefore it prevents the inclusion of 3D cylinders. This limitation presents two potential solutions: transitioning CoastalFOAM to a 3D model or employing an alternative method for incorporating vegetation characteristics. This thesis focuses on maintaining the 2D framework due to the established validated 2D-vertical model and known computational costs associated with modeling vegetation as cylinders within a 3D OpenFOAM model.

CoastalFOAM has been validated for simulating 2D flow through a rock filter layer, the rock filter layer is hereby modelled as a porous layer (Jacobsen et al., 2017). This capability allows the model to calculate the wave energy dissipation in these layers. While the model can calculate changes in flow velocity within the porous layer, a key limitation exists. The existing method is specifically designed for stone layers. The problem is that the wave attenuation due to a vegetated foreshore needs to be calculated.

1.3. Objective and research questions

The objective of this thesis is to simulate wave attenuation by salt marsh vegetation using the model CoastalFOAM. Once validated, this model will make it possible to calculate wave overtopping or wave loads on dikes fronted by salt marsh vegetation on the foreshore.

The main research question of the thesis is:

'How can a porous layer within CoastalFOAM be used to model wave attenuation during storm conditions by salt marsh vegetation at the foreshore of a dike?'

The main research question is broken down into smaller questions, each aimed at providing a detailed exploration of specific parts. The sub-questions of this research are:

1. What experimental conditions and wave attenuation measurements are needed to calibrate the CoastalFOAM model for simulating wave attenuation by salt marsh vegetation?
2. How to apply the method to calculate porous media flow through a stone layer to simulate the wave attenuation by a salt marsh?
3. What differences exist in the calculated wave attenuation between the physical flume experiment and the CoastalFOAM flume experiment?

1.4. Thesis outline

This thesis delves into the theoretical background in chapter 2, equipping the reader with the knowledge necessary for subsequent chapters. Chapter 3 describes the case study. Chapter 4 then discusses the methodology, which describes all the steps necessary to answer the main research question. The next step is to set up the CoastalFOAM model, which is described in chapter 5. The method in combination with the model set up is used to come to results, which are shown in chapter 6. The results are discussed in chapter 7. Finally, chapter 8 draws conclusions based on the research, and chapter 9 offers recommendations for further research.

2

Theoretical Background

2.1. Sea waves

Sea waves are disturbances that travel across the ocean's surface. These disturbances can be caused by wind blowing over the water, earthquakes, or gravitational forces from the moon and sun. This thesis is focused on wind waves which have typical wave lengths between 1 and 1000 meter and wave periods between 1 and 30 seconds (van der Werf, 2022). As the wave travels, the water itself does not actually move forward, but rather rises and falls in a circular motion. Figure 2.1 shows the dimensions of an idealized regular surface wave, and the terminology used for describing the waves.

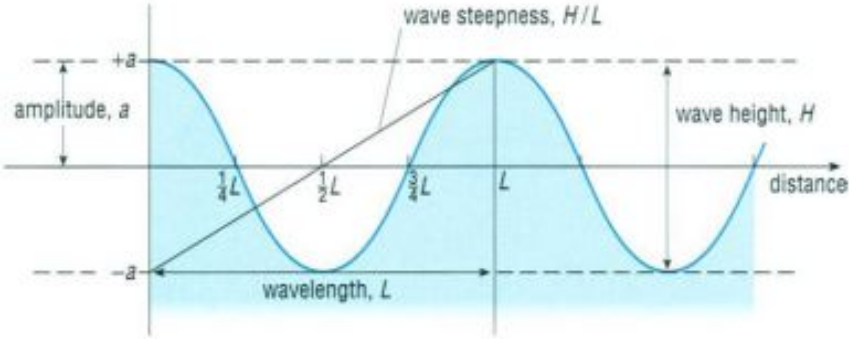

Figure 2.1: Vertical profile of two successive idealized ocean waves (The Open University, 1999)

It illustrates that surface waves follow a sinusoidal motion. The wave height (H) represents the vertical distance between the wave trough (lowest point) and the wave crest (highest point). It is important to note that the wave height is twice the amplitude. The wave length (λ) is the horizontal distance between two successive crests (or troughs) of the wave. The wave period (T) refers to the time interval between two successive crests (or troughs) passing a fixed point. The frequency (f) represents the number wave peaks (or troughs) that pass a fixed point per second.

Wind speed, wind duration, and fetch length all influence wave characteristics, resulting in a range of irregular waves. Figure 2.2 shows an example of such a wave field.

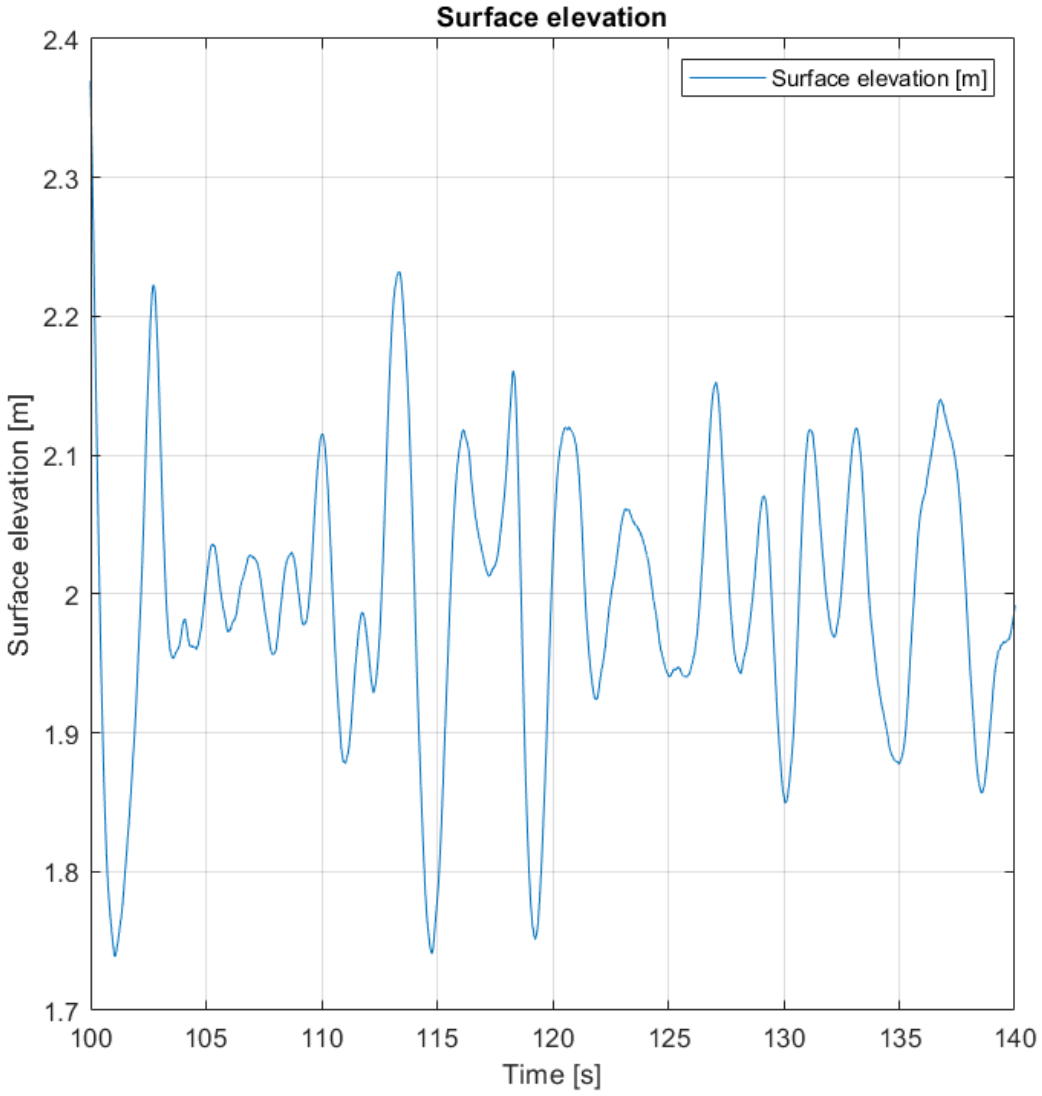

Figure 2.2: Schematization of an irregular wave

Fourier transforms reveal how wave characteristics, including wave energy, are distributed across different wave frequencies, creating a wave spectrum. JONSWAP (Joint North Sea Wave Project) spectrum is such a spectrum. The variation in wave characteristics makes waves irregular. Unlike regular waves, which have a single frequency and a consistent pattern, irregular waves consist of a statistical approximations of many waves with different frequencies and wave heights to determine standard wave characteristics. Wave characteristics such as: peak wave period (T_p), zeroth moment wave height (H_{m0}), and the root mean square wave height (H_{rms}). Figure 2.3 shows a wave spectrum with the corresponding peak wave period (T_p).

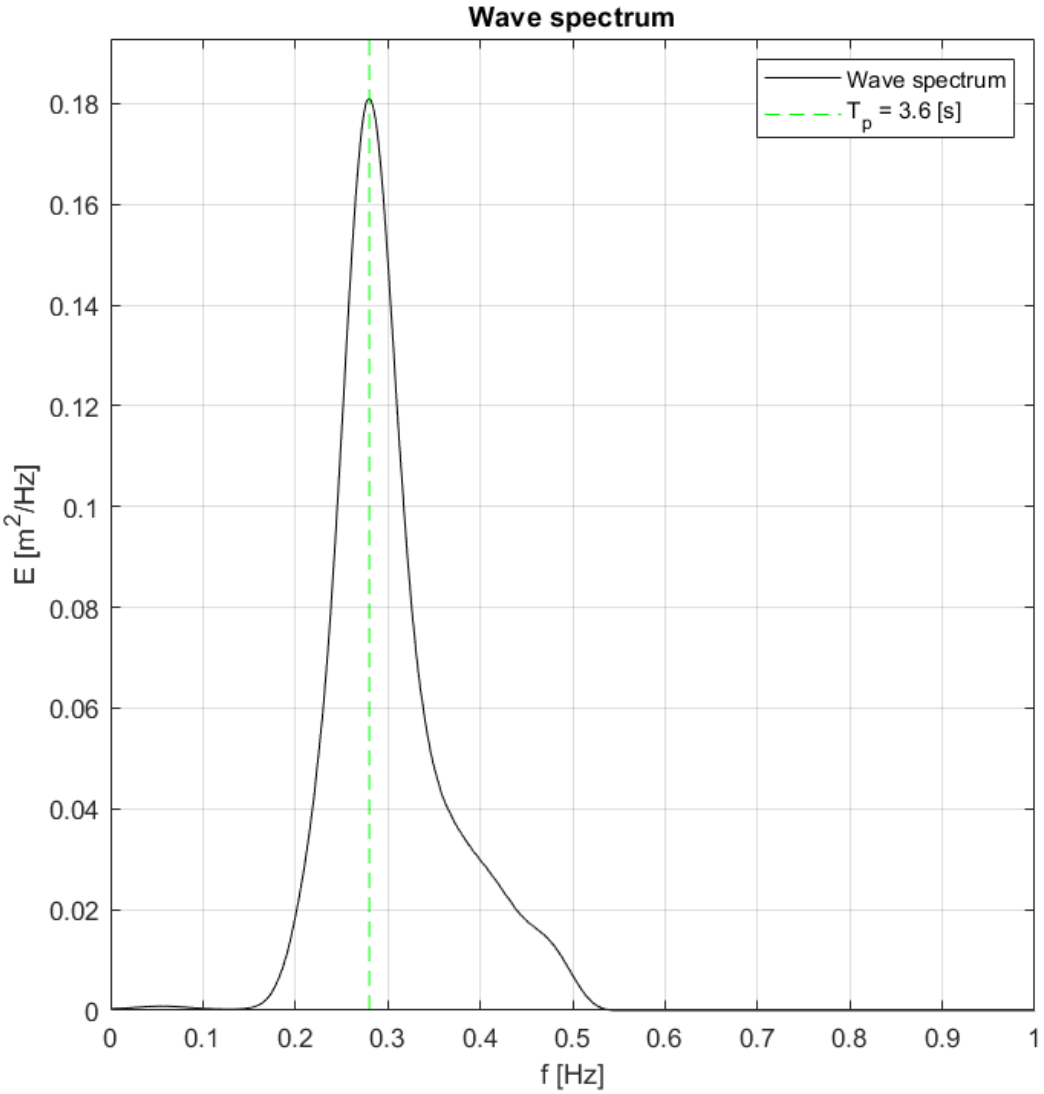

Figure 2.3: Schematization of a wave spectrum

The zeroth moment wave height (H_{m0}) can be calculated with equation 2.1. The root mean square wave height (H_{rms}) can be calculated with respectively equation 2.2 (Möller et al., 2014).

$$H_{m0} = 4\sqrt{m_0} \tag{2.1}$$

m_0 is the zeroth moment of the wave spectrum. m_0 represents the total energy content of the wave field and is calculated by integrating the spectral density function over the frequencies.

$$H_{rms} = \sqrt{\frac{1}{N_i}\sum_{i=1}^{N} H_i^2} \tag{2.2}$$

N_i is the number of incident waves and H_i the individual wave height in the time series of incident waves.

Figure 2.4 shows the orbital patterns of a surface wave. The orbital patterns in deep water trace nearly circular paths with the largest orbital diameters at the surface, matching the wave height. These diameters decrease as water depth increases, becoming negligible by half the wavelength. In contrast, shallow water forces the orbits to become progressively flattened as waves interact with the seabed. Intermediate water depths present a mix of these behaviors, with orbital shapes transitioning from circular towards flattened as the seabed's influence becomes more significant.

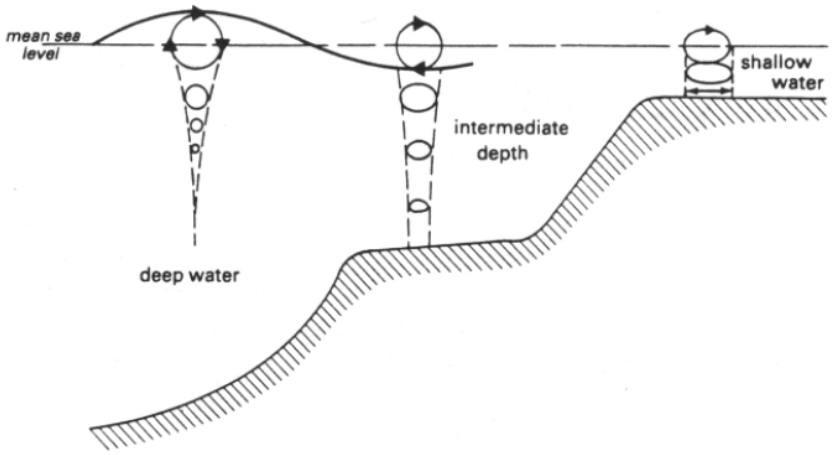

Figure 2.4: Schematization of the change of the orbital velocity with water depth (The Open University, 1999)

The orbital velocities can be calculated with equation 2.3.

$$u(z) = \pi \frac{H_{m0}}{T_p \sinh(\frac{2\pi z}{\lambda})} \tag{2.3}$$

z is the coordinate vector in the direction of the water column. For equation 2.3, z represents the distance between the water level and the depth where the orbital velocity needs to be determined.

2.2. Salt marshes

Coastal salt marshes may broadly be defined as coastal areas, vegetated by herbs, grasses or low shrubs (Esselink et al., 2017). Salt marshes provide multiple ecosystem services such as: wave attenuation, biodiversity support, carbon sequestration and can prevent erosion (Brooks et al., 2023; Hughes, 2004; Vázquez-Lule and Vargas, 2021).

The presence of a salt marsh can disturb the orbital velocity of waves, as shown in figure 2.5. Consequently, this disturbance leads to a reduction in the wave's orbital velocity, which in turn affects wave characteristics such as period, height, and length.

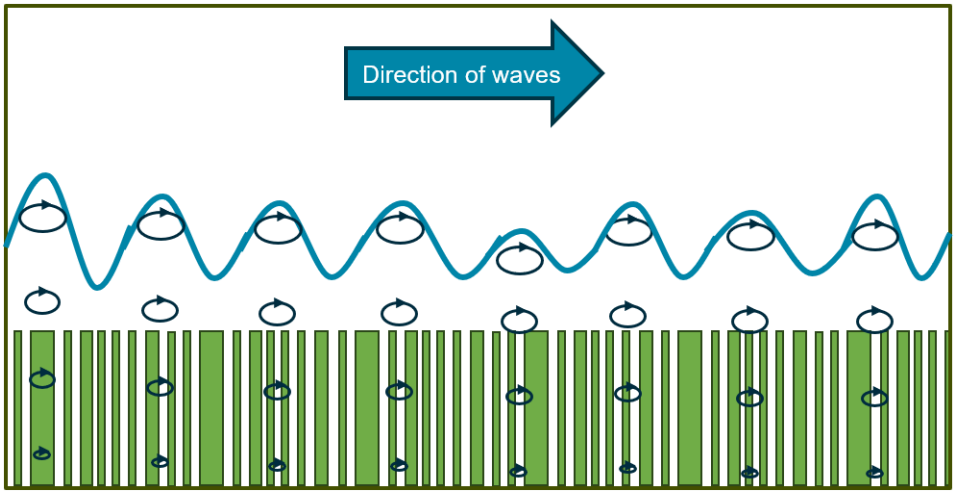

Figure 2.5: Schematization of the orbital velocity above a salt marsh in intermediate water

Salt marshes typically flourish in estuaries or intertidal environments, which means they are subjected to periodic flooding (tidal and non-tidal). Figure 2.6 shows the salt marsh exist of different plant species along the cross section of a salt marsh. The water depth rises or falls with the tides, the size of the difference in water depth varies per zone.

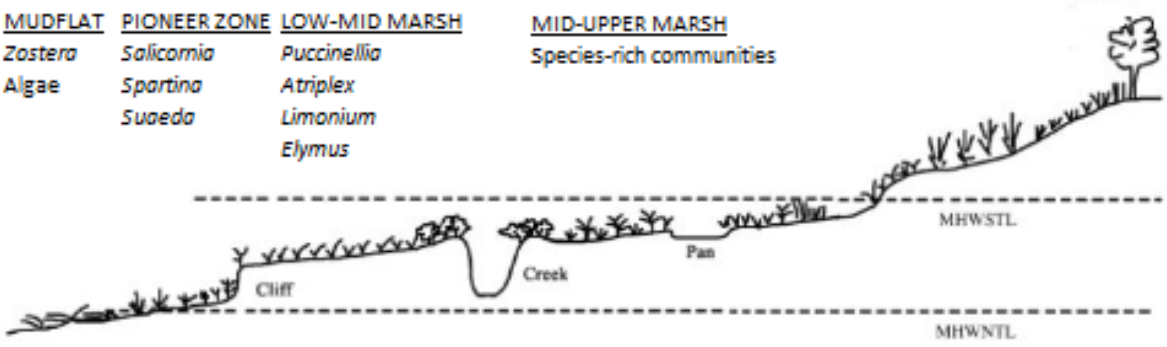

Figure 2.6: Cross section of a typical northwest European salt marsh, illustrating the relative positions of some of the most abundant species (Hughes, 2004)

Foreshores consisting of both bare tidal flats and vegetated salt marshes are well studied for their wave attenuating capacity, and can serve as add-on to conventional coastal defenses (Willemsen et al., 2020). Salt marshes can dissipate wave energy due to the bottom profile and vegetation (Vuik et al., 2016b). Salt marshes have high potential for a contribution to coastal protection, despite the uncertainty as a consequence of using vegetation and thereby introducing intrinsic biological uncertainties (Bouma et al., 2014).

Vegetation characteristics, including the flexibility of vegetation and its seasonal variation, play a role in influencing the wave attenuation capacity of salt marshes (Vuik et al., 2016b; Zhu et al., 2023). Figure 2.7 shows the seasonal change between winter and summer of perennial grasses. The aboveground standing biomass and vegetation stiffness are both key drivers in wave attenuation (Paul et al., 2016). There are many types of grasses, such as these two typical salt marsh species *Elymus athericus* (highly flexible) and *Spartina alterniflora* (relatively rigid) (Zhu et al., 2023). The results of van Veelen et al. (2020) show that flexible vegetation attenuates waves up to 70% less than rigid vegetation due to swaying of flexible plants. These biological factors must be carefully considered when integrating salt

marshes as natural add-on to conventional coastal defense strategies.

Figure 2.7: Seasonal change of a salt marsh between winter and summer (Vuik et al., 2016b; Zhu et al., 2023)

2.3. Modelling sea waves and vegetation

In order to describe the water motion of wind-generated waves in the vertical x-z plane, the two-dimensional (2D-vertical) Reynolds-Averaged Navier-Stokes (RANS) equations and the continuity equation can be used. Flow uniformity is hereby assumed in the lateral y-direction (van der Werf, 2022). Due to the complexity of solving the RANS equations, simplifications are often made, leading to analytical solutions. However, Computational Fluid Dynamics (CFD) can solve the Navier-Stokes equations directly. This offers an advantage over analytical solutions because it can handle complex geometries and multi-phase flows (air-water). This allows more accurate modelling of highly nonlinear effects such as wave breaking (Karola et al., 2024).

In order to describe the wave attenuation by a salt marsh, the vegetation is in many studies simplified by describing its structure with a few key parameters to represent the vegetation as rigid cylinders (Mullarney and Henderson, 2018). These parameters are listed below and schematized in figure 2.8.

- Stem diameter (S_d)
- Stem height (S_h)
- Stem density (S_n)
- Space between stems (ΔS)
- Length of the salt marsh in the direction of the propagation of the wave (L)

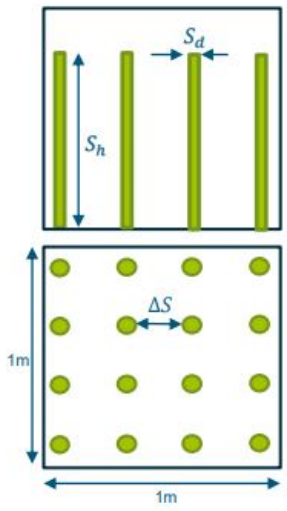

Figure 2.8: Schematization of vegetation characteristics

The drag equation is used to calculate the resistance force due to the cylinders. Equation 2.4 shows the drag equation.

$$F_x = \frac{1}{2}\rho C_d S_d S_N |u| u \tag{2.4}$$

In this equation u is the horizontal velocity in the vegetation region due to the wave motion, S_d is the plant stem diameter, S_n is the number of vegetation stems per unit horizontal area, and C_d is a depth-averaged drag coefficient. The drag coefficient accounts for among others things the shape of the grass and the roughness of the blades of the grass. In addition, the drag coefficient covers the ignorance of the plant motion in this formula (Mendez and Losada, 2004).

2.4. CoastalFOAM

JIP(Joint-Industry-Project) CoastalFOAM is a validated RANS CFD numerical wave flume model, which is a model developed by Royal HaskoningDHV, Deltares, Boskalis, and van Oord. CoastalFOAM is built in OpenFOAM. The model in OpenFOAM consists of a module for wave generation (waves2FOAM). Waves2FOAM makes it possible to generate a wind induced wave spectrum, with the following spectral shapes JONSWAP and Pierson-Moskowitz (Jacobsen et al., 2017). CoastalFOAM is validated for simulating wave overtopping, wave loads on crest walls, and it is proven to be effective in simulating flow through rubble mount structures (Boersen et al., 2019; Jacobsen et al., 2017, 2018). The stones of the rubble mount structure are modelled in CoastalFOAM as one porous layer, and therefore it is not necessary to model every stone separately.

2.5. Porous layer

The wave damping effect of salt marsh vegetation will be integrated into CoastalFOAM by modeling the vegetation as a porous layer. Equation 2.5 shows the momentum equation for porous media flows. It is a modified version of the Navier-Stokes equations to account for the flow through a permeable structure.

$$(1 + C_m)\left(\frac{\partial}{\partial t}\right)\left(\frac{\rho u}{n_p}\right) + \frac{1}{n_p}\nabla\left(\frac{\rho}{n_p}\right) uu^T = -\nabla\rho^* + gx\nabla\rho + \frac{1}{n_p}\nabla\cdot(\mu_u \nabla u) - F_p \tag{2.5}$$

With C_m the added mass coefficient, t time, $/rho$ the density of the fluid, n_p the porosity of the permeable structure, p^* an excess pressure, g the gravitational acceleration vector, x the Cartesian coordinate vector, μ_u the dynamic viscosity of the velocity field and F_p takes into account the resistance of the permeable structure on the flow (Boersen et al., 2019).

The porous layer approach, which is the resistance term, in CoastalFOAM is used to design for example rubble mount structures (Jacobsen et al., 2017). Breakwaters often utilize layers of stones, with larger stones placed on the outer layer for increased stability (Figure 2.9). The risk of wave-induced erosion depends on the orbital flow velocity of the water. To analyze this flow velocity reduction through the breakwater, the stone layer is modelled as a porous layer. This simplification allows for calculations of the decreasing orbital velocity within the layers. The study Boersen et al. (2019) shows that the model can simulate wave overtopping over a breakwater, resulting from a decrease in wave height due to stone layers modelled as porous layers.

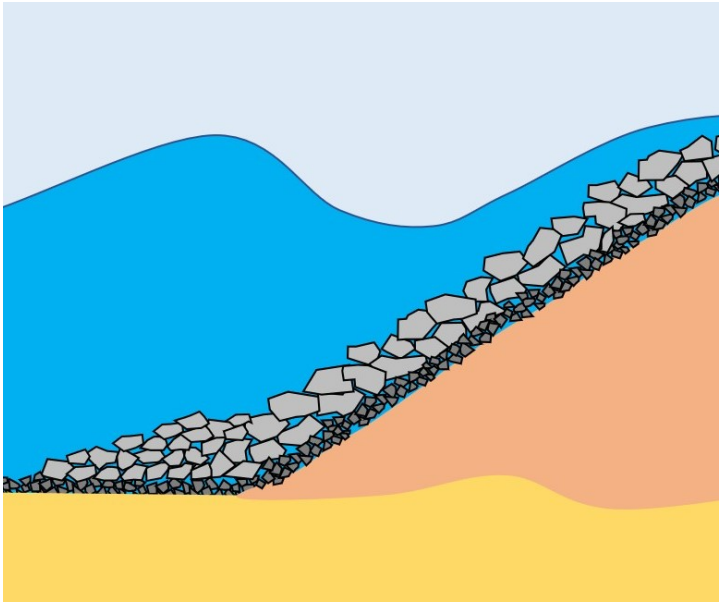

Figure 2.9: Cross section of breakwater (Dronkers, 2020)

The resistance term is calculated in CoastalFOAM with the Darcy-Forchheimer equation, which is adjusted for a rock layer. The equation is shown in equation 2.6. This equation's initial component, based on Darcy's law, describes a linear relationship for laminar flow. As the Reynolds number increases, flow transitions from this laminar regime to a turbulent regime. To account for this non linearity, Forchheimer introduced an additional term to capture the growing influence of inertial effects at higher fluid velocities (Ghasemi et al., 2023).

$$F_p = a\rho u + b\rho||u||u \tag{2.6}$$

The equation incorporates separate terms for the resistance force. Coefficients a and b, determined by equations 2.7 and 2.8 respectively, govern these resistance forces. ρ is the density of water and u is the horizontal flow velocity in the direction of the propagation of the wave.

$$a = \alpha \frac{(1-n_p)^2}{n_p^3} \frac{\nu}{D_{50}^2} \tag{2.7}$$

$$b = \beta \left(1 + \frac{7.5}{KC}\right) \frac{1-n_p}{n_p^3} \frac{1}{D_{50}} \tag{2.8}$$

ν is the kinematic molecular viscosity, D_{50} is the nominal diameter of the permeable layer, n_p is the porosity of the rock layer, KC is the Keulegan-Carpenter number, and α and β are closure coefficients. The standard values for α and β are respectively 1000 and 1.1, but (Jensen et al. (2014)) showed that the same results can be obtained with interchanged values of α and β. The values of α ranges from 0

to 3000 and the value of β from 0.5 to 4. The KC value is set to 10000 in the paper of Boersen et al. (2019), which reflects the assumption of minimal influence of the KC-number.

In the current model, the porous layer has been established for a rock layer. The characteristics of this layer are defined by two parameters:

- Porosity of Stones (n_p): This can be calculated using equation 2.9 (Schiereck and Verhagen, 2012).
$$n_p = 1 - (\rho_b/\rho_s) \tag{2.9}$$
With ρ_b the dry bulk density and ρ_s the soil particles density.
- Median Grain Size of stones (D_{50}): This can be measured using techniques such as sieve tests.

To determine the applicability of the Darcy-Forchheimer equation (2.6) for a specific flow scenario in porous media, the porous Reynolds number needs to be calculated. This dimensionless parameter, obtained using equation 2.10, characterizes the relative importance of α and β. As shown in table 2.1 the value of the porous Reynolds number determines the flow regime (Jensen et al., 2014).

$$Re_p = \frac{\overline{u} D_{50}}{n_p \nu} \tag{2.10}$$

$\overline{u}$ is the flow velocity averaged per time step and over each control volume (Moretto, 2019).

Table 2.1: Darcy-Forchheimer flow regimes based on porous Reynolds rumber

Regime	Flow regime	Range Re_p	α and β
Darcy laminar flow regime	Laminair flow	1 <Re_p<10	α=? and β=0
Darcy-Forchheimer flow regime	Transitional flow	10 <Re_p<300	α=? and β=?
Fully turbulent flow regime	Fully turbulent flow	Re_p>300	α=0 and β=?

3

Case study

3.1. Selection case study

The important hydrodynamic conditions and vegetation characteristics discussed in chapter 2 are summarized here for convenience, because they form the basis of the research method.

The following hydrodynamic conditions must be considered for this research:

- Time series of the water surface elevation before and after the salt marsh or calculated significant wave heights (H_{m0}) and wave periods (T_p)
- Water depth (h)

The following listed vegetation characteristics must be considered for this research:

- Stem diameter (S_d)
- Stem height (S_h)
- Stem density (S_N)
- Length of the salt marsh in the direction of the propagation of the wave (L)

Two case studies were selected that meet the stated requirements. These case studies are named 'Project Bassia' and 'Project BE SAFE' and are respectively detailed in appendix A and appendix B. Although both were considered, the advantages of the flume experiment called 'Project Bassia' from Möller et al. (2014) led to the selection of this case study. The 'Project Bassia' case study was chosen for this research due to its use of a flume experiment. This controlled environment allows for a direct comparison with the numerical model by eliminating external factors such as wind and alongshore currents. This setup is ideal for an initial test of the feasibility of modeling wave attenuation by vegetation in CoastalFOAM. While the BE SAFE project, with its varying water levels, would have offered additional calibration opportunities. The 'Project Bassia' study offers valuable calibration cases for both vegetation characteristics and hydrodynamic conditions. The vegetation characteristics are modified by mowing the grass, while the hydrodynamic conditions are altered by adjusting the wave height and wave period.

3.2. Project Bassia: flume experiment

The experiment was conducted in a 310 meter long, 5 meter wide, and 7 meter deep wave flume. Figure 3.1 shows an outline of the experiment in a part of the flume. The length of the experiment is 60 meter with wave gauges in front and after the vegetation. The vegetation has a length of 40 meter. The distance from the wave paddle to the vegetation is 108 meter (Rupprecht, 2015).

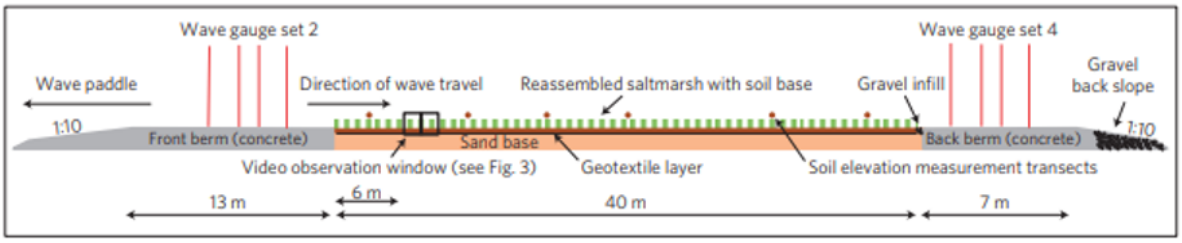

Figure 3.1: Flume experiment (Möller et al., 2014)

The exact position of the wave gauges in the flume from the wave paddle are shown in table 3.1. The wave gauges in the first and second set of instruments are numbered.

Table 3.1: Location wave gauges in the flume

Name	WG 2.1	WG 2.2	WG 2.3	WG 2.4
Location [m]	99.32	101.39	102.94	104.52
Name	WG 4.1	WG 4.2	WG 4.3	WG 4.4
Location [m]	148.62	150.69	152.24	153.82

The vegetation characteristics of the salt marsh are known and shown in table 3.2. The vegetation in the flume consists of three types of vegetation as described in D. *Elymus athericus* is the dominant vegetation type and in the paper of Möller et al. (2014), the calculation of the vegetation drag coefficient is only based on the value of this vegetation type. The same assumption will be made for this research and therefore the drag force due to the other vegetation types will be neglected.

Table 3.2: Vegetation characteristics of *Elymus athericus* in the flume

	S_h[m]	S_d $[mm]$	S_n $[stems/m^2]$
Elymus athericus	0.7	1.3	1700

The research by Möller et al. (2014) provides data on various hydrodynamic conditions, including root mean square wave height (H_{rms}) and the peak wave period (T_p). The chosen cases are shown in table 3.3 and a complete overview of all performed tests can be found in appendix A.

Table 3.3: Selected tests from the study of Möller et al., 2014

Test date & Number	Named	T_p $[s]$ Front	H_{rms} $[m]$ Front	H_{rms} $[m]$ Back
20131021_6	Wave-1	3.6	0.571	0.470
20131022_4	Wave-2	5.1	0.602	0.510
20131031_9	Wave-1-mowed	3.6	0.573	0.523

The test '20131021_6' is selected as the base case and named Wave-1. The reasons for selecting this test as the base case are listed below:

- Wave Height: The wave height for this test is relatively high, making it suitable for investigating wave attenuation effects during storms. Higher wave heights allow for clearer quantification of the differences in wave attenuation behaviour.
- Mesh Size: The relatively large wave height also allows for a coarser mesh, which can significantly reduce computational time.

- Wave Period: The wave period for this test is relatively low compared to other higher wave conditions. This translates to shorter simulation times, as the simulation duration is dictated by the number of waves simulated.
- Non-breaking waves: The waves must remain non-breaking in the flume. The tests with higher significant wave heights have individual waves that will break. The occurrence of breaking waves at higher significant wave heights complicates the analysis, as breaking is also a damping mechanism.
- Higher Wave Option: The availability of a test with a higher wave condition '20131022_4' ,called Wave-2, further supports the choice for this test. With the same mesh size, a higher wave condition would yield even more accurate results, eliminating the need for mesh refinement.
- Mowed case Availability: A case with mowed grass '20131031_9' is available for this test and named Wave-1-mowed, providing an opportunity to investigate changes in vegetation characteristics by changing the vegetation height.

The root mean square wave height (H_{rms}) is given. However, for the CoastalFOAM model, the significant wave height (H_{m0}) is required. By analyzing the time series of the physical flume test and CoastalFOAM in the same way, a direct comparison can be made between CoastalFOAM and the flume experiment. The significant wave height will be determined as the zero moment wave height (H_{m0}), explained in section 2.1. The calculation of the wave spectra, peak wave period (T_p) and significant wave height (H_{m0}) is shown in section 3.3.

3.3. Analysis Case study

The water surface elevation timesries of the flume tests Wave-1, Wave-2 and Wave-1-Mowed are analyzed to determine the significant wave height (H_{m0}), peak wave period (T_p) and wave spectra. The significant wave height (H_{m0}) and peak wave period (T_p) are necessary as input for the CoastalFOAM model. The time series for Wave-1 at wave gauge 2.1 is shown in figure 3.2.

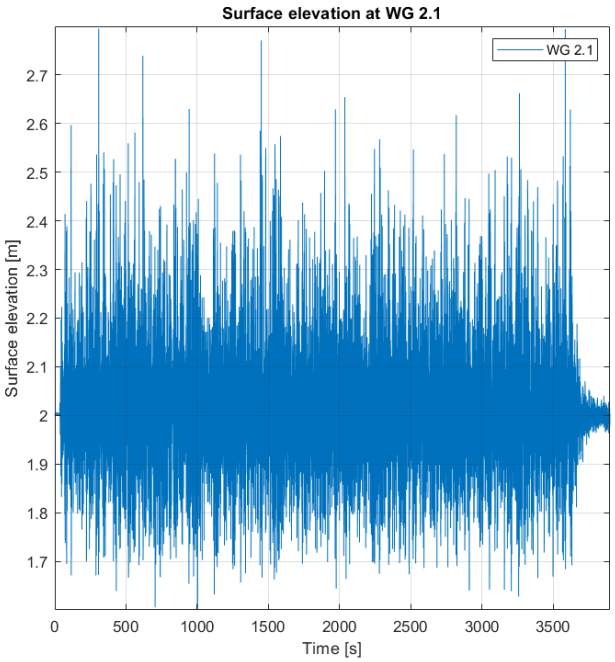

Figure 3.2: Time series at WG 2.1 for Wave-1

The figure shows that there are almost no variations in water surface elevation in the first 100 seconds of the wave and last 200 seconds. Therefore those parts of the time series are not taken into account

for the calculation of the hydrodynamic conditions. The maximum number of waves is used to achieve the closest possible approximation of the actual H_{m0} value, and therefore 3600 seconds which is about 1000 waves are used to approximate the hydrodynamic wave conditions for Wave-1. The same approach is used for the other wave conditions that are selected. The results are shown in table 3.4. Wave-1-mowed is also analyzed for 1000 waves and Wave-2 is analyzed for about 960 waves.

Table 3.4: Hydrodynamic conditions of the physical flume experiment

Test name	Vegetation	T_p $[s]$	H_{m0} $[m]$	$Hm0$ $[m]$	T_p $[s]$	Reduction H_{m0} [%]
		Front	Front	Back	Back	Front to back
Wave-1	Vegetation	3.56	0.582	0.493	3.57	18.1
Wave-2	Vegetation	5.14	0.624	0.548	5.17	13.9
Wave-1-mowed	Mowed	3.56	0.590	0.549	3.57	7.5

Figure 3.3 shows the wave spectra for the selected tests. The red line represents the wave spectra before reaching the vegetation, while the black line shows the spectra after the wave interaction with the vegetation. The figure clearly demonstrates that most of the wave energy loss occurs in the higher frequency range, indicating that shorter wave periods experience more damping. The difference in wave energy reduction between Wave-1 and Wave-1-mowed is also clearly visible.

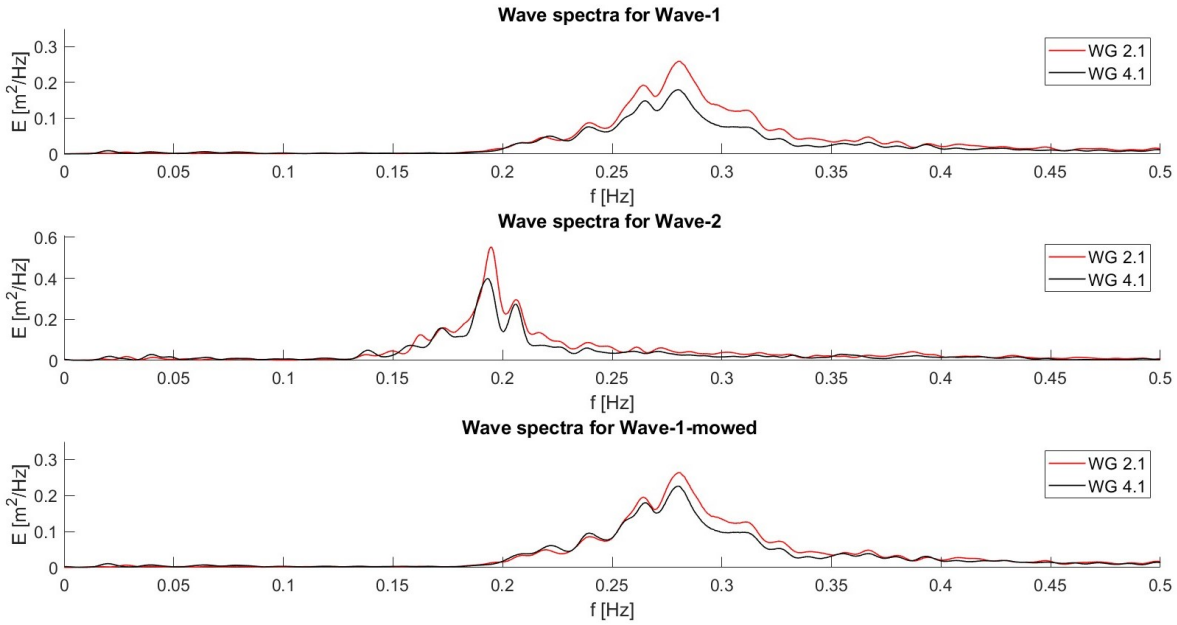

Figure 3.3: Comparison between wave spectra before and after the vegetation for the physical flume experiment

4

Method

4.1. Conversion vegetation characteristics to model input

This section describes a newly developed method for converting vegetation characteristics into input parameters for a porous layer in the CoastalFOAM model. Figure 4.1 illustrates the process of converting 3D structures, such as stones or salt marshes, into a simplified porous layer suitable for model input.

Figure 4.1 shows the conversion process in four steps. The first step is a side view of the 3D structure. The second step, labeled 'frontal area', presents a cross-section perpendicular to the wave direction of the 3D structure. The third step, 'averaged frontal area', demonstrates how the stone layer can be described using parameters like D_{50} and n_p, while a salt marsh is characterized by parameters S_d, S_h, and S_N. The parameters are described in section 2.2 and 2.5. Finally, the last step removes the width of the model, resulting in a 2D vertical model.

The method for converting from step 3 to step 4 (averaged frontal area to model input) is known for stones (as described in Section 2.5), but remains unknown for salt marshes. The main reason for this is because stones have a spherical shape and grass stems have a cylindrical shape. This section will elaborate on the main research gap.

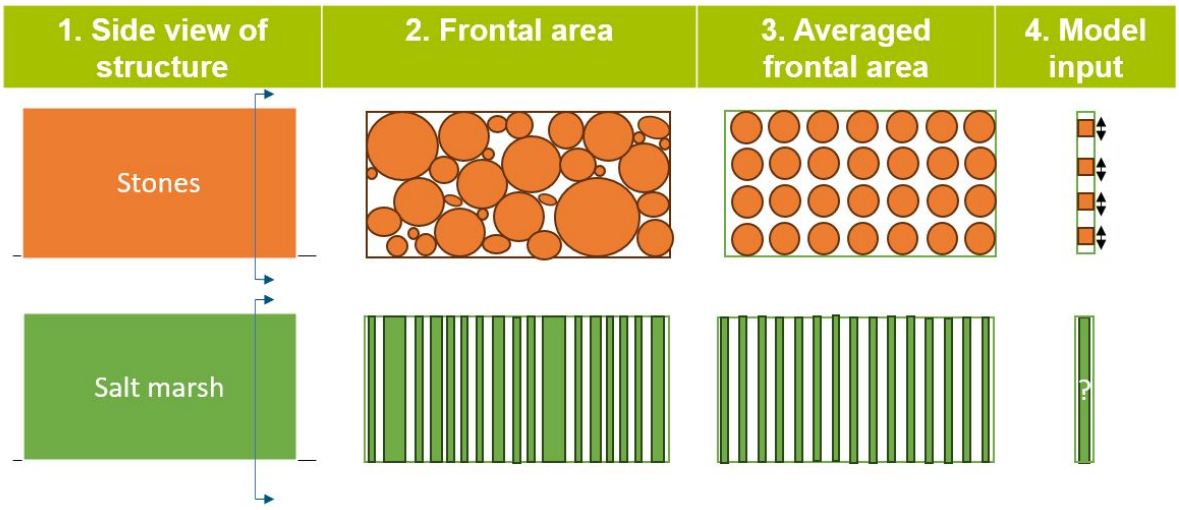

Figure 4.1: Overview of the conversion of stone parameters in to salt marsh characteristics

The two parameters which quantify the dimensions of the porous layer for stones are D_{50} and n_p. This

are the first parameters to convert.

The porosity of a stone layer is represented by a dimensionless number, indicating the fraction of space occupied by water or air (not stones). This concept can be extended to vegetation using equation 4.1 (Yin et al., 2023a).

$$n_p = V_t - V_v/V_t \tag{4.1}$$

In equation 4.1, V_v is the volume of the vegetation which can be calculated with equation 4.2. The volume of the vegetation is calculated with a fixed diameter and height. This equation therefore assumes that the vegetation consists of straight rigid cylinders. This simplification can result in overestimating or underestimating of the wave attenuation due to the simplification of the grass structure, which is discussed in section 4.2

$$V_v = S_h S_N \pi (S_d/2)^2 \tag{4.2}$$

V_t is the total volume and can be calculated with equation 4.3. The total volume is limited by the stem height because the porous layer represents only the volume occupied by the stems. Both equations (4.2 and 4.3) include the height of the vegetation, so the height could be eliminated and the outcomes will be the same.

$$V_t = A_v S_h \tag{4.3}$$

A_v is vegetated area.

In a stone layer, the median grain size (D_{50}) dictates the size of the pores. Since grain size and pore size are typically in the same range, the median grain size can be considered equivalent to the width of the open spaces (van Heest, 2022). Consequently, for vegetation, the distance between plant stems (ΔS) is adopted for the median grain size (D_{50}). Equation 4.4 details the calculation of this inter-stem spacing (Mullarney and Henderson, 2018).

$$\Delta S = S_N^{-1/2} - S_d \tag{4.4}$$

The derivation of equations 4.1 and 4.4 provides a methodology for transforming vegetation properties into a porous layer representation. This methodology enables the determination of both the porosity (N_p) and median grain size (D_{50}) of the porous layer.

To determine the applicability of the Darcy-Forchheimer equation 2.6 for a specific flow scenario in porous media, the porous Reynolds number needs to be calculated. For convenience, This part is repeated here from section 2.5 as this is an important part of conversion of the vegetation characteristics. This dimensionless parameter, obtained using equation 4.5, characterizes the relative importance of α and β. The relative importance between those calibration parameters is explained in section 2.5. As shown in table 2.1 the value of the porous Reynolds number determines the flow regime (Jensen et al., 2014).

$$Re_p = \frac{\overline{u} D_{50}}{n_p \nu} \tag{4.5}$$

$\overline{u}$ is the flow velocity averaged per time step and over each control volume (Moretto, 2019). The calculation of the average velocity will be simplified in this research. The oscillating velocity at the bottom

will be used as a approximation of the averaged flow velocity in the porous layer. The general equation to calculate the orbital velocity is shown in equation 4.6.

$$u(z) = \pi \frac{H_{m0}}{T \sinh(\frac{2\pi z}{\lambda})} \tag{4.6}$$

The equation is explained in section 2.1. The value of z will therefore be equal to the water depth.

Boersen et al. (2019) employed a KC-number of 10000 in their study, assuming minimal influence of this parameter on the simulated processes. This simplification applies to a stone layer, where equation 2.8 shows that a higher KC-number reduces the resistance force in the Darcy-Forchheimer equation. However, for models involving vegetation, numerous studies have established relationships between the drag force exerted by vegetation and the KC-number (Haddad et al., 2024; Liu et al., 2023; Yin et al., 2023b). The KC-number will therefore be reintroduced in CoastalFOAM. Equation 4.7 shows the equation of the KC-number (Jensen et al., 2014).

$$KC = \frac{u_m T_p}{n_p D_{50}} \tag{4.7}$$

The maximum oscillating velocity u_m is assumed for simplification to be the same as the orbital velocity at the bottom. Section 7.3 of the discussion will elaborate on the KC number.

While a method now exists to calculate the resistance force using all relevant parameters, two coefficients, α and β, remain undetermined. These parameters require calibration with the CoastalFOAM model.

4.2. Assumptions

This section details the assumptions made during the conversion process of the vegetation characteristics (section 4.1) and the assumptions required for the model setup (section 4.3). The vegetation assumptions are the same assumptions that are made in the paper of Möller et al. (2014).

Vegetation assumptions

- Simplified grass vertical layer: The actual grass-like shape of the vegetation is simplified to a cylindrical shape in the model. Figure 4.2 shows a picture of *Elymus athericus*, which reveals that the plant's structure varies along its height. This assumption can underestimate the damping effect of the model, because the upper part of the stems seems to have a less cylindrical shape.
- Uniform Stem Height: All stems in the model are assumed to have the same height. This may lead to an underestimation of the damping effect in the model, as it could result in reduced turbulence and consequently lower form drag compared to a more realistic vegetation canopy with varying stem heights.
- Rigid Stems: The stems are assumed to be rigid and not bend. This neglects swaying motion and inertial forces. The damping effect is likely overestimated, as flexible stems attenuate waves less effectively, as detailed in section 2.2.
- Undamaged Vegetation: The model assumes the vegetation remains undamaged. However, according to Möller et al. (2014), the vegetation was damaged during tests with relatively high waves. Consequently, this assumption may lead to an overestimation of wave attenuation, as the modeled vegetation does not account for this damage.
- Focus on *Elymus athericus*: The model considers only the dominant species, *Elymus athericus*, excluding other vegetation types that might also influence wave attenuation on a smaller scale. This assumption may lead to an underestimation of wave attenuation, as the modeled vegetation does not fully represent the existing vegetation.

- Uniform Stem Distribution: The model assumes vegetation stems are uniformly distributed. However, wave attenuation can be influenced by vegetation patches, as described in Maza et al. (2016).

Figure 4.2: *Elymus athericus* (Rupprecht, 2015)

Model Assumptions

- Vertical damping: The porous layer provides the same wave energy damping in the direction of the propagation of the wave (x) as the vertical direction (z). Grasses do not have the same geometry in all directions, like stones. However, wave energy damping in the vertical direction is considered negligible due to low orbital velocities in the vertical direction. Figure 4.3 shows the orbital velocity in x and z direction in an empty flume in CoastalFOAM. The graph shows orbital velocities at a specific point along the x-axis, coinciding with wave crest formation. It reveals that for lower z-coordinate values, the orbital velocity in the z-direction remains minimal. However, as the z-coordinate increases, the orbital velocity in the z-direction also rises. It is important to note that this could potentially include air velocity components as well.

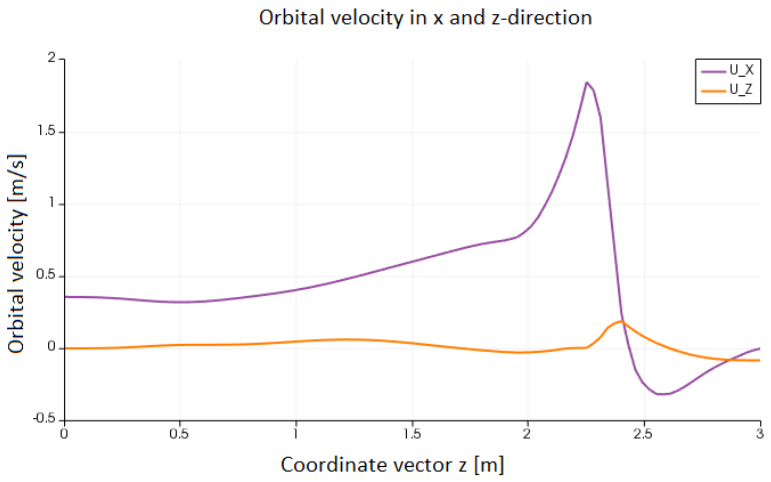

Figure 4.3: Orbital velocites in x and z-direction

- Bottom roughness is incorporated within the porous layer: The numerical wave flume is assumed to have negligible wave attenuation in the absence of a porous layer. Therefore, bottom roughness is not incorporated as a boundary condition in the model. Instead, the porous layer captures the combined effect of vegetation drag and bed roughness.
- Simplified Turbulence Representation: Turbulence is not explicitly modeled in this approach, no use was made of a turbulence model. Instead, the porous layer captures the combined effect of vegetation drag and the associated turbulence generation. As described in section 2.5, the Forchheimer term becomes increasingly significant at higher velocities incorporating the effects of turbulence.
- Negligible wave reflection within the flume: The flume's outlet is equipped with a relaxation zone to reduce wave reflection, allowing the assumption of negligible wave reflection within the flume.
- 2D vertical is the same as 3D: It is assumed that 2D vertical processes replicate 3D behavior and therefore wave energy dissipation in the direction perpendicular to the wave propagation can be neglected. This assumption may overestimate the porous layer's damping capacity due to the absence of transverse energy losses.

4.3. CoastalFOAM settings

4.3.1. Geometry

The geometry of the flume is based on the flume experiment as shown in figure 3.1. The model is shortened to reduce computation time, because a flume experiment in CoastalFOAM is always set up as shown in figure 4.4. The model consists in this figure of four different zones: left relaxation zone, generation zone, impact zone, and the relaxation zone (Horstman, 2020). At the end of the wave generation zone, the waves are fully developed.

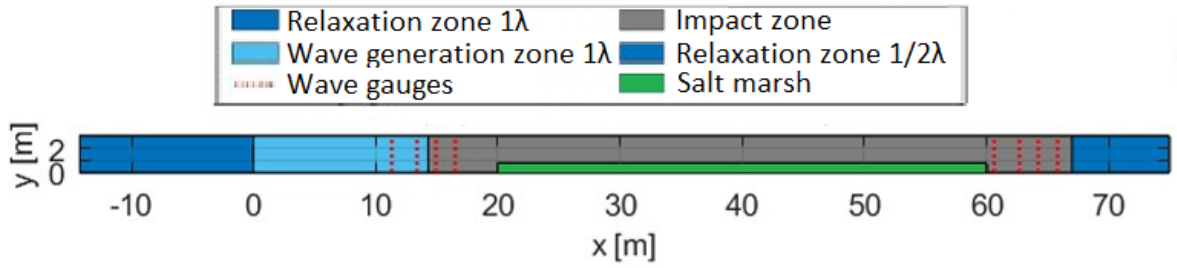

Figure 4.4: Numerical model set-up Wave-1

The length of the zones is based on the wavelength. The wavelength (λ) can be determined by an iterative process using equation 4.8.

$$\lambda = \lambda_0 \tanh\left(\frac{2\pi h}{\lambda}\right) \tag{4.8}$$

The deep water wave length (λ_0) can be calculated with equation 4.9.

$$\lambda_0 = \frac{gT_p^2}{2\pi} \tag{4.9}$$

Wave gauges are placed before and after the vegetation to measure the water surface elevation. The wave gauge sets exist of four wave gauges for reflection analysis. In this model it is assumed that there is no wave reflection because of the relaxation zone, therefore minimum wave reflection is expected. For optimal results, gauges should be positioned at two key points: the end of the wave development zone (capturing fully developed waves) and after the vegetation, but before the relaxation zone (avoiding its wave-dampening effect). The location of the wave gauges should be based on the distance from the start and end of the salt marsh. This precise placement ensures accurate measurement of wave attenuation by the salt marsh vegetation. CoastalFOAM can be used to determine the significant wave height (H_{m0}) at these positions with the use of equation 2.1).

4.3.2. Mesh

The mesh for this model is 2D vertical, with Blockmesh defining the base mesh size. SnappyHexMesh then allows for localized refinement within the Blockmesh. This function effectively subdivides each cell in the refinement region into four cells of equal size.

A crucial step of the model setup is selecting the appropriate mesh size. A common rule of thumb in CoastalFOAM suggests using one-tenth of the significant wave height (H_{m0}) as cell size. Additionally, a refinement zone around the water level is used with a size of two times H_{m0}. Two times H_{m0} serves as an estimate for the maximum wave height (He et al., 2023). This refinement ensures accurate representation of wave dynamics in the critical near-surface region. The mesh around the refinement can be coarser due to this refinement, which reduces the computation time. To analyze how vegetation (the porous layer) affects sea waves, the mesh within the vegetated area is also refined with respect to the Blockmesh from the bottom to the height of the flume using SnappyHexMesh. This increased resolution is intended to better model the interaction between waves and the porous layer, including the crucial orbital velocities within the water column.

The mesh size needs to be tested to see if the model input matches with the model results. Finer meshes in CFD models are crucial for accurate wave heights. Coarser meshes cause numerical dispersion, which could result in the model simulating lower waves. Therefore a range Blockmesh sizes will be tested, this includes both finer and coarser cells compared to the one-tenth significant wave height (H_{m0}) rule. The entered H_{m0} will be measured after the wave development zone to confirm if it matches the model input. The significant wave height at this point should not deviate by more than 5% from the entered value. Additionally, the decrease in wave height without a porous layer along the flume should be minimal, and should not be more than 5%. In this way, the wave attenuation will fully caused by the porous layer. This process of testing different mesh sizes is crucial for finding the optimal balance between computational efficiency and accuracy.

4.3.3. Model runtime

The model runtime will be determined based on the peak wave period of the incoming waves. As described in Section 2.1, both the significant wave height and peak wave period represent statistical

approximations of real-world, irregular wave conditions. To accurately capture these characteristics within the simulation, CoastalFOAM requires a minimum of 300 waves to make a good estimation of the significant wave height based on experts knowledge.

To account for the flume's warm-up period, the model will be run for a duration that allows the initial waves to travel the entire flume length. This ensures that the simulated water surface elevation reflects the behavior of fully developed waves within the flume. Equation 4.10 can be used to calculate the required computation time (T_c) based on T_p and the flume length.

$$T_c = \frac{L_f}{\lambda} T_p \tag{4.10}$$

with L_f the numerical wave flume length.

4.4. Calibration and sensitivity analysis

4.4.1. Calibration of the model

The number of calibration parameters required will be determined based on the porous Reynolds number as outlined in section 4.1. The calibration process will adapt to the number of parameters needed. The values of the calibration parameters α, β or both needs to be obtained. Wave-1 will serve as the base case. To establish initial values for α, β, or both, equations 2.6 and 2.4 will be compared. The value of the resistance force needs therefore be the same for both equations. The model will be run for various values of α, β, or both to determine the optimal values by a fitting process.The fitting process will minimize the percentage difference in wave attenuation between the physical flume experiment and CoastalFOAM results. This will result in a calibrated base case where the percentage reduction in significant wave height matches that of the physical flume experiment.

4.4.2. Sensitivity analysis

The results for the sensitivity analysis will include the change in significant wave height, the change in peak wave period, and the change in wave spectra between the PFE and CFE.

The calibrated base case model will now be tested against changes in hydrodynamic conditions and vegetation characteristics, these two scenarios are listed below:

- Wave-2 : The simulation will be conducted with an increase in significant wave height and peak wave period to investigate the model's ability to calculate wave attenuation under a variation in hydrodynamic conditions. The KC number will increase due to the stronger oscillatory flow (higher T_p and H_{m0}). This increase might cause a reduction of the wave attenuation capacity of the salt marsh at higher wave heights and with longer peak wave periods. Because a higher KC value will reduce the resistance force.
- Wave-1-mowed: The simulation will be conducted with a decrease in stem height to investigate the model's ability to calculate wave attenuation under a variation in vegetation characteristics. The bending of the vegetation is less for vegetation with a lower height. The question therefore arises if the wave attenuation will indeed be underestimated, when only the vegetation height is changed.

5

Model set up

5.1. Conversion vegetation characteristics to model input

Wave-1 serves as the base test for the conversion process, with subsequent tests acting as variations on this initial configuration for sensitivity analysis. Table 5.1 summarizes the key vegetation characteristics and hydrodynamic conditions relevant to Wave-1, Wave-2 and Wave-1-Mowed summarizing information from both sections 3 and 3.3.

Table 5.1: Vegetation characteristics and hydrodynamic conditions for Wave-1, Wave-2 and Wave-1-mowed

Wave 1		**Wave 2**		**Wave-1-mowed**	
Vegetation characteristics		Vegetation characteristics		Vegetation characteristics	
S_d $[m]$	0.013	S_d $[m]$	0.013	S_d $[m]$	0.013
S_N $[m^{-2}]$	1700	S_N $[m^{-2}]$	1700	S_N $[m^{-2}]$	1700
S_h $[m]$	0.7	S_h $[m]$	0.7	S_h $[m]$	**0.05**
Hydrodynamic conditions		Hydrodynamic conditions		Hydrodynamic conditions	
H_{m0} $[m]$	0.582	H_{m0} $[m]$	**0.624**	H_{m0} $[m]$	0.582
T_p $[s]$	3.6	T_p $[s]$	**5.1**	T_p $[s]$	3.6
h $[m]$	2	h $[m]$	2	h $[m]$	2
ρ $[kg/m^3]$	1000	ρ $[kg/m^3]$	1000	ρ $[kg/m^3]$	1000
ν $[m^2/s]$	1E-6	ν $[m^2/s]$	1E-6	ν $[m^2/s]$	1E-6

The conversion method described in section 4.1 is now used to transform the information in table 5.1 to the model input in table 5.2.

Table 5.2: Model input for Wave-1, Wave-2 and Wave-1-mowed

Wave 1		**Wave 2**		**Wave-1-mowed**	
V_t [m^3]	0.7	V_t [m^3]	0.7	V_t $[m^3]$	**0.05**
V_v [m^3]	1.6E-3	V_v $[m^3]$	1.6E-3	V_v $[m^3]$	**1.12E-4**
n_p [-]	0.998	n_p [-]	0.998	n_p [-]	0.998
D_{n50} $[m]$	0.023	D_{n50} $[m]$	0.023	D_{n50} $[m]$	0.023
λ $[m]$	14.29	λ $[m]$	**21.42**	λ $[m]$	14.29
u_{max} $[m/s]$	0.509	u_{max} $[m/s]$	**0.619**	u_{max} $[m/s]$	0.509
Re_p [-]	11717	Re_p [-]	**14242**	Re_p [-]	11717
KC [-]	80	KC [-]	**138**	KC [-]	80

The results indicate that the porous Reynolds number is more than an order of magnitude higher than the limiting value of 300. According to Table 2.1, this implies that α is equal to zero. Consequently, equation 2.6 can be simplified to the form shown in equation 5.1, where the influence of the viscous term is negligible.

$$F_p = \rho\beta\left(1 + \frac{7.5}{KC}\right)\frac{1-n_p}{n_p^3}\frac{1}{D_{50}}||u||u \tag{5.1}$$

All but the calibration coefficient, β, are now known parameters in equation 5.1.

5.2. CoastalFOAM settings

5.2.1. Geometry

The geometry of the numerical wave flume is explained in section 4.3.1 and figure 2.8 already showed the geometry for Wave-1 and Wave-1-mowed. The only difference for Wave-1-mowed is that the height of the porous layer, which represents the salt marsh, is lower. Figure 5.1 shows the numerical wave flume for Wave-2. Compared to the numerical flume of Wave-1, the relaxation and wave generation zones are longer.

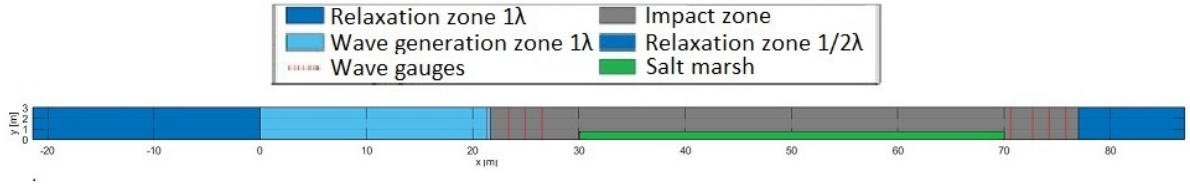

Figure 5.1: Numerical model set-up wave-2

5.2.2. Mesh

For Wave-1 the significant wave height is equal to 0.582 meter, the block mesh has therefore a cell size of approximately 0.058 meter and a refinement between 1.4 and 2.6 meter. To reduce computation time, the possibility of using a coarser mesh was investigated. The following block mesh sizes were tested: 0.05, 0.075, 0.1, and 0.2 meter. The number of waves that are tested for the mesh size are 100.

The first step is to test if the significant wave height just after the wave development zone does not deviate by more than 5% in the model compared to the entered value. To manage computation time a preliminary analysis will be conducted using 100 waves. Table 5.3 indicates a reduction in computational time when increasing the mesh size from 0.05 to 0.075 meter but also a decrease in accuracy. While accuracy showed minimal variation between mesh sizes of 0.075 and 0.1 meter, computational time decreased by an additional 9 hours. A mesh size of 0.2 meter resulted in a significant wave height deviation exceeding 5%. Consequently, a mesh size of 0.1 meter was selected for waves equal to or larger than 0.58 meter, as larger waves need larger mesh sizes. Appendix C provides a detailed analysis of mesh selection and its impact on wave height reduction along the flume.

Table 5.3: Determine block meshsize

Block meshsize [m]	Percentage difference H_{m0} [%]	Computation time [hours]
0.05	2.78	58
0.075	4.08	14
0.1	4.85	5
0.2	6.12	2

The second step involves verifying that the significant wave height decreases by no more than 5%

between the first and second wave gauge sets. To ensure meaningful results, this test utilizes the base case numerical wave flume and a simulation duration of 300 waves matching the final run conditions. Table 5.4 confirms a significant wave height reduction of 1.1%, indicating mesh suitability.

Table 5.4: Change in hydrodynamic conditions of wave-1 empty flume (300 waves)

Test name	T_p $[s]$	H_{m0} $[m]$	H_{m0} $[m]$	T_p $[s]$	Reduction H_{m0} [%]
	Front	Front	Back	Back	Front to back
Wave-1 empty flume	3.58	0.566	0.560	3.62	1.1

Figure 5.2 shows a schematic representation of the mesh of a part of the numerical wave flume. The bigger cell sizes have a size of 0.1 meter, and the refinement region has a cell size of 0.05 meter. As a general rule of thumb, a mesh size approximately one-tenth of the significant wave height should be used within the refinement zone, while the overall Blockmesh size can be approximately one-fifth of the significant wave height.

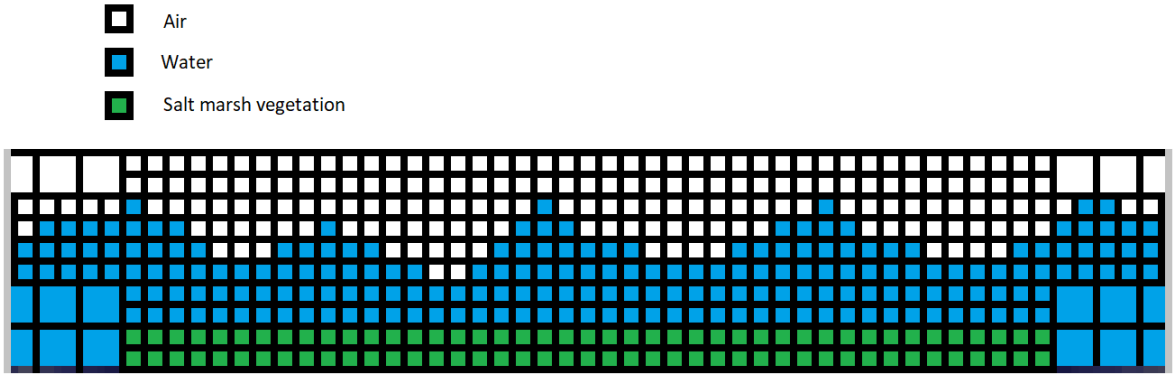

Figure 5.2: Schematization of mesh around the salt marsh vegetation

5.2.3. Model runtime

The warm-up period can be calculated according to section 4.3 for 300 waves and is for Wave-1 and Wave-2 respectively equal to 20 and 30 seconds. Appendix D describes in general the CoastalFOAM model that is built in OpenFOAM and the total runtime of the model for the different tests.

5.3. Calibration of the model

The calibration process will focus on Wave-1 conditions. Equation 5.1 presents the simplified formula for calculating the porous layer's resistance force, derived through substitution. To approximate the calibration parameter β, equation 5.1 will be compared to equation 2.4, which represents the resistance force calculated using the drag equation approach for cylindrical elements. The resistance force for both equation will be calculated for various flow velocities (u) to approximate the value of β. However, equation 2.4 lacks a value for the drag coefficient (C_d). The value of C_d is determined in the paper of Möller et al. (2014) and equal to 0.349.

By plotting both equations in MATLAB and seeking for a complete similarity of both results, a first approximation is obtained for β. Figure 5.3 shows this concept, with the red dashed line representing the approximation using equation 5.1 and the blue dotted line for equation 2.4.

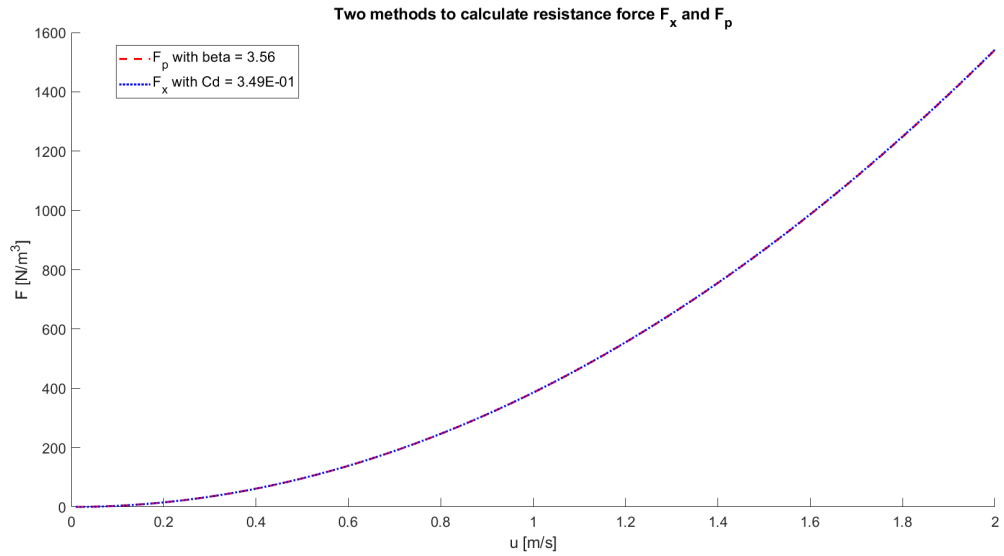

Figure 5.3: Approximation of β by a comparison between F_x and F_p

Based on the previously determined β using equations 5.1 and 2.4, a value of 3.56 was obtained. This falls within the calibration range as in the paper of Jensen et al. (2014). The following β values are used 2, 3, 4 and 5, and the resulting percentage wave height reduction for each β is shown in table 5.5 and plotted in figure 5.4. A linear regression analysis yields a high r^2 value of 0.9995, indicating a strong linear relationship. As Table 3.4 shows, the desired wave height reduction for Wave-1 is 18.1%. The intersection point between the fitted line and the 18.1% reduction line in figure 5.4 provides a calibrated β value of 4.84. This value will be used for Wave-1 in further analyses for β.

The two methods used to determine β yield different results. The method comparing the two equations underestimates the calibration coefficient required in CoastalFOAM. Section 4.2 indicates that this difference may be due to the porous layer needing to account for both the damping effect due to turbulence and bottom roughness. This requirement was not present in the model based on cylinders combined with the drag force equation.

Table 5.5: Reduction in H_{m0} for the range of β values for Wave-1

Beta	H_{m0} $[m]$ Front	H_{m0} $[m]$ Back	Reduction [%] Front to Back	Range of time $[s]$
2	0.564	0.521	8.3	20-1100
3	0.564	0.504	11.9	20-1100
4	0.562	0.488	15.2	20-1100
5	0.561	0.473	18.6	20-1100

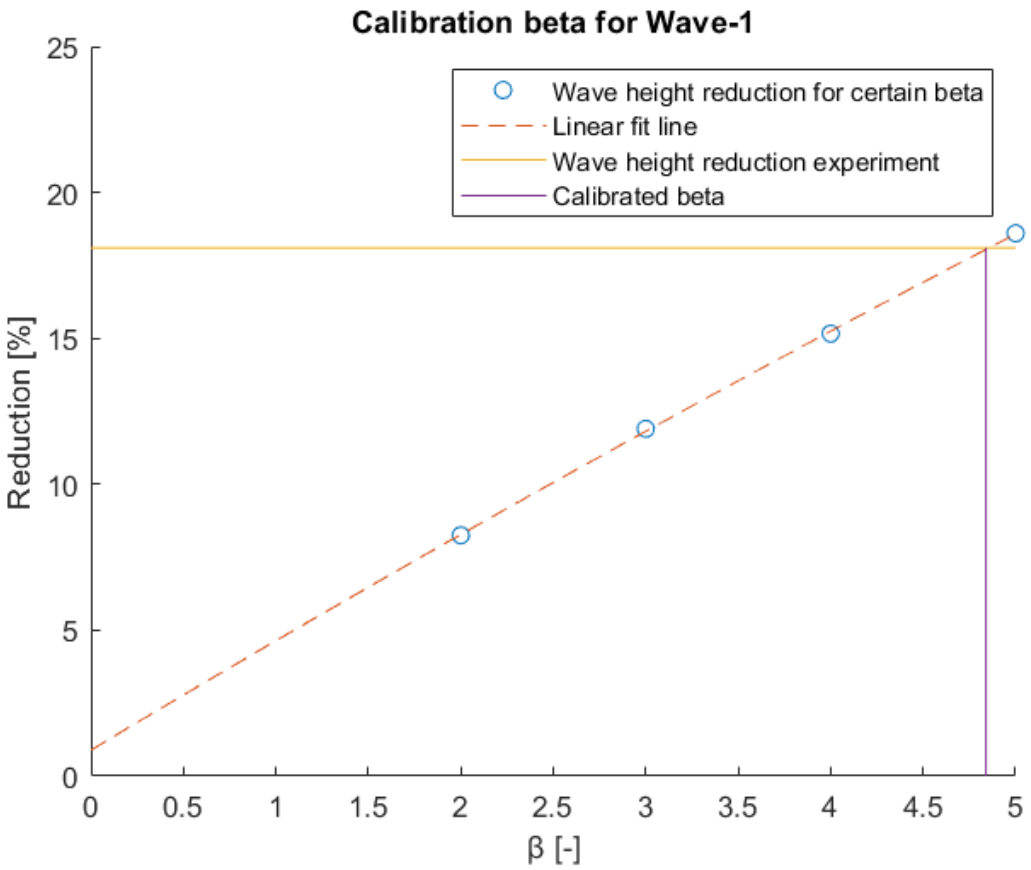

Figure 5.4: Calibration of the value of β for Wave-1

The calibrated value of β has now been incorporated in the CoastalFOAM model. The resulting wave height reduction is 18.4% for 300 waves. While this value differs slightly from the expected reduction of 18.1%, this difference might be attributed to rounding errors in β.

6

Results

6.1. Base case (Wave-1)

Table 6.1 shows the results from the CoastalFOAM flume experiment (CFE) and repeats the results for the physical flume experiment (PFE) from section 3.3. The Wave-1 test case has been tested with 300 waves, resulting in a 18.4% reduction in wave height. This results in a 1.65% difference in wave attenuation between the calibrated beta run for Wave-1 and the physical flume experiment. The peak wave period (T_p) increased in time by 0.56% in the CFE and by 0.28% in the PFE. This increase is not significant for both tests, the CFE and the PFE.

Table 6.1: Wave-1 comparison H_{m0} and T_p for PFE and CFE

Test name	T_p [s]	H_{m0} [m]	H_{m0} [m]	T_p [s]	Reduction H_{m0} [%]
	Front	Front	Back	Back	Front to back
Wave-1 CFE	3.58	0.561	0.474	3.60	18.4
Wave-1 PFE	3.56	0.582	0.493	3.57	18.1

Figure 6.1 compares the change before and after the vegetation of the wave spectra for CFE and PFE. It is visible that the CFE like the PFE, effectively dampens shorter wave periods more clearly than longer waves. This phenomenon was already mentioned in section 3.3 and is also visible in CoastalFOAM.

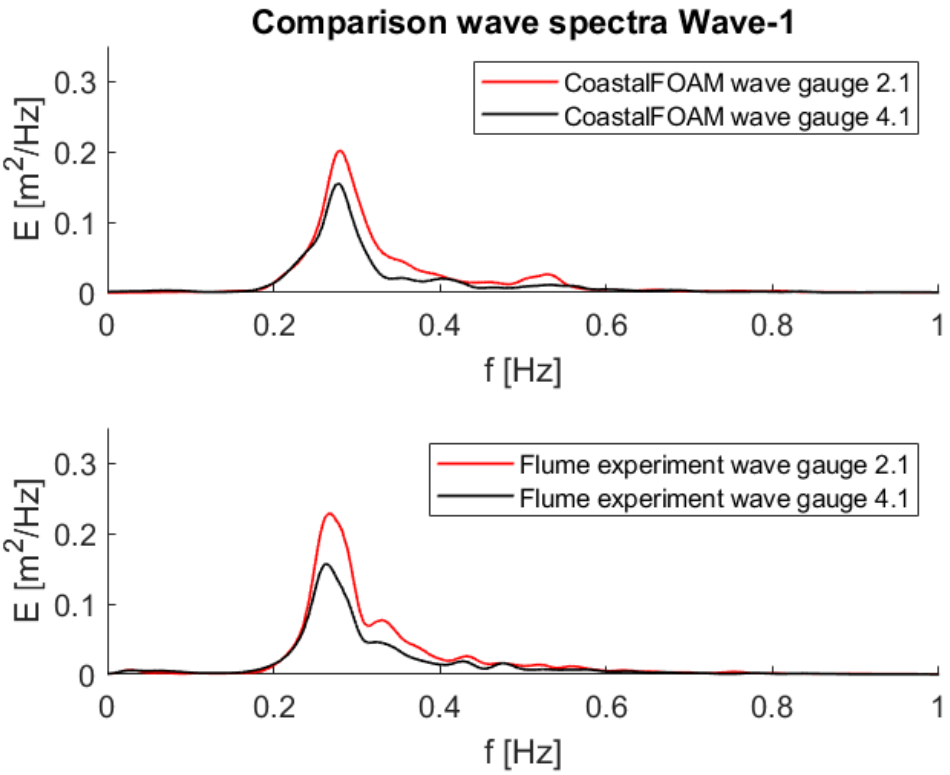

Figure 6.1: Wave-1 spectra comparison: CFE vs. PFE

Figure 6.2 compares the wave spectra from CoastalFOAM simulations with the physical flume experiment. The spectra show close agreement, indicating that CoastalFOAM accurately captures the wave characteristics.

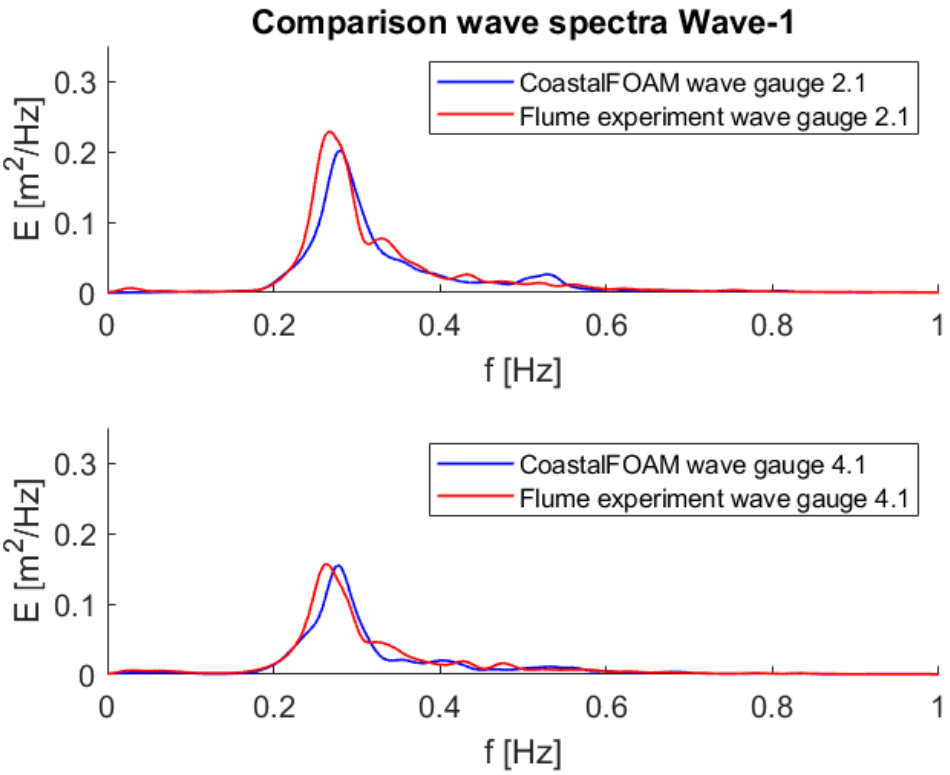

Figure 6.2: Wave-1 spectra comparison: CFE vs. PFE before and after the salt marsh

6.2. Higher wave (Wave-2)

Table 6.2 shows the change in significant wave height (H_{m0}) and the peak wave period (T_p) for Wave-2. The CFE overestimates the wave height reduction by more than 10%. This difference is significant, as it exceeds the 5% accuracy threshold determined in Section 5.2.2. Consequently, the porous layer overestimates the resistance force for the salt marsh vegetation for the wave-2 conditions. The peak wave period remains unchanged for both CFE and PFE.

Table 6.2: Wave-2 comparison H_{m0} and T_p for PFE and CFE

Test name	T_p [s]	H_{m0} [m]	H_{m0} [m]	T_p [s]	Reduction H_{m0} [%]
	Front	Front	Back	Back	Front to back
Wave-2 CFE	5.12	0.597	0.483	5.12	23.6
Wave-2 PFE	5.14	0.624	0.548	5.17	13.9

Figure 6.3 compares the change before and after the vegetation of the wave spectra for CFE and PFE. Wave energy reduction occurs at unexpected frequencies. Notably, the CFE exhibits the most pronounced damping around 0.4 Hz, while the PFE at approximately 0.2 Hz.

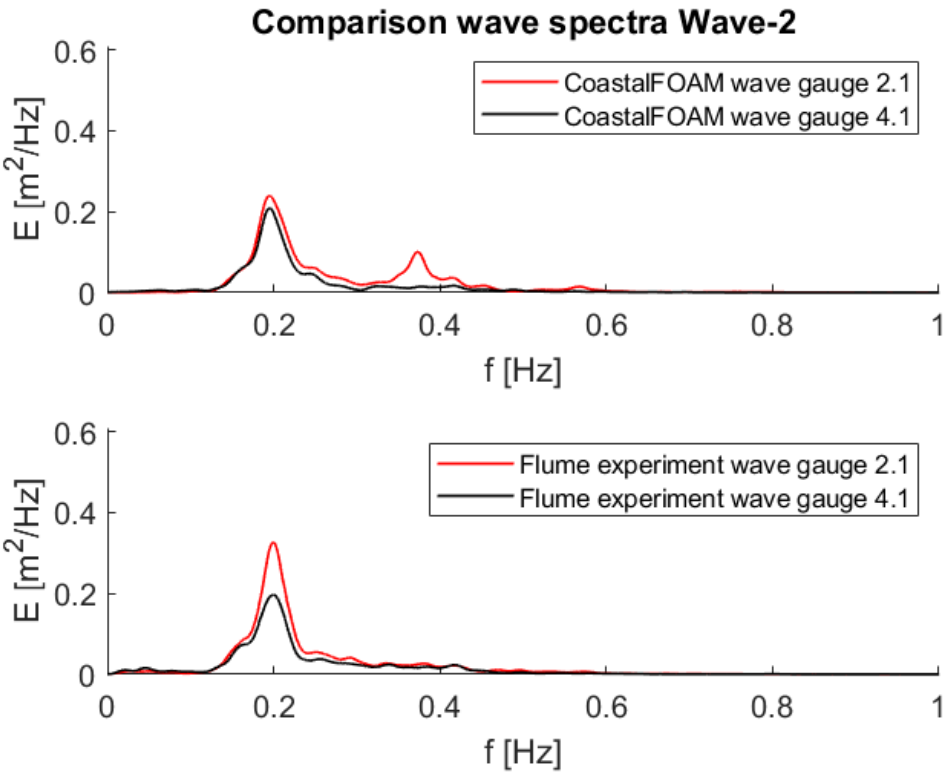

Figure 6.3: Wave-2 spectra comparison: CFE vs. PFE

Figure 6.4 compares the wave spectra from the CFE with the PFE. It indicates that the wave spectra from CoastalFOAM, even in front of the salt marsh, does not align with the wave spectra obtained from the physical flume experiment. Specifically, CoastalFOAM underestimates the peak wave energy around 0.4 Hz and overestimates the wave energy around 0.2 Hz. Wave spectra downstream of the vegetation align again between the PFE and CFE.

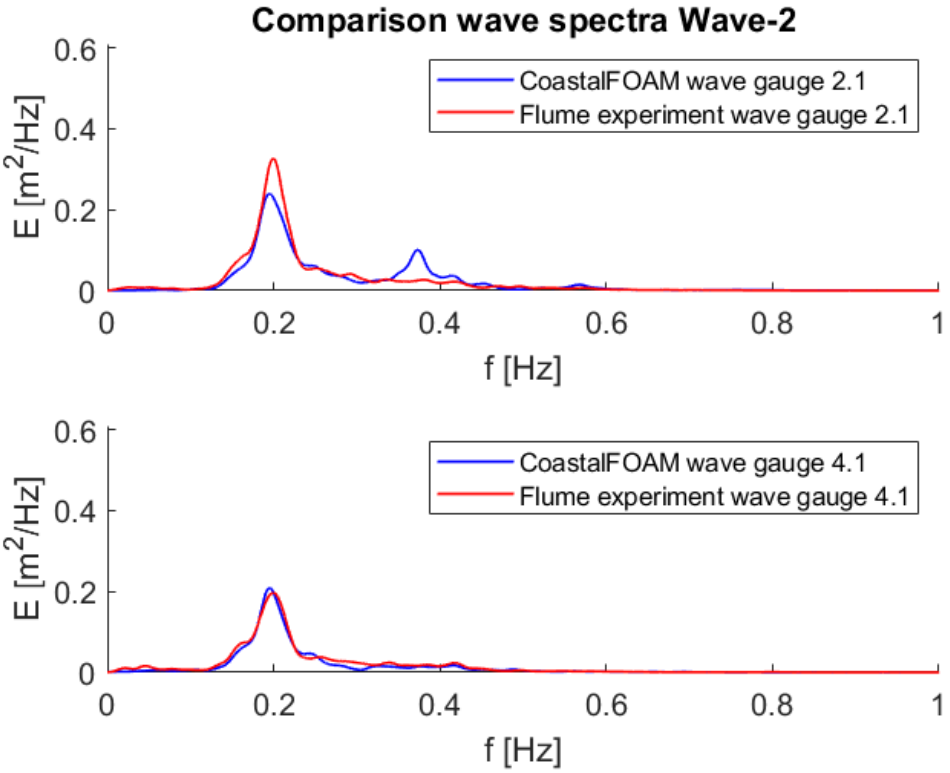

Figure 6.4: Wave-2 spectra comparison: CFE vs. PFE before and after the salt Marsh

Table 6.3 shows a reduction of the β by making a comparison with the study of Möller et al. (2014). The study shows a decrease in C_d for wave-2 compared to wave-1. The C_d value for respectively wave-1 and wave-2 are equal to 0.349 and 0.299. The percentile decrease is equal 16.7, the same decrease for β results in a value of 4.15 for wave-2 instead of 4.84 for wave-1. Table 6.3 shows still a significant overestimation of the damping effect of the porous layer for the vegetation for wave-2 conditions.

Table 6.3: Wave-2 comparison H_{m0} and T_p for PFE and CFE

Test name	T_p [s]	H_{m0} [m]	H_{m0} [m]	T_p [s]	Reduction H_{m0} [%]
	Front	Front	Back	Back	Front to back
Wave-2 CFE β=4.15	5.09	0.594	0.495	5.05	20
Wave-2 PFE	5.14	0.624	0.548	5.17	13.9

6.3. Lower vegetation height (Wave-1-mowed)

Table 6.4 shows the change in significant wave height (H_{m0}) and the peak wave period (T_p) for Wave-1-mowed. The CFE underestimates the wave height reduction, which was expected to be 7.5%, but the model predicted a reduction of only 2.5%. This difference is significant, as it exceeds the 5% accuracy threshold established in section 5.2.2. Consequently, the porous layer underestimates the resistance force for the salt marsh vegetation for the wave-2 conditions. The peak wave period remains unchanged for both CFE and PFE.

Table 6.4: Wave-1-mowed comparison H_{m0} and T_p for PFE and CFE

Test name	T_p [s]	H_{m0} [m]	H_{m0} [m]	T_p [s]	Reduction H_{m0} [%]
	Front	Front	Back	Back	Front to back
Wave-1-mowed CFE	3.58	0.568	0.554	3.61	2.5
Wave-1-mowed PFE	3.56	0.590	0.549	3.57	7.5

Figure 6.5 compares the change before and after the vegetation of the wave spectra for CFE and PFE. The figure reveals a generally lower energy reduction for CFE compared to PFE.

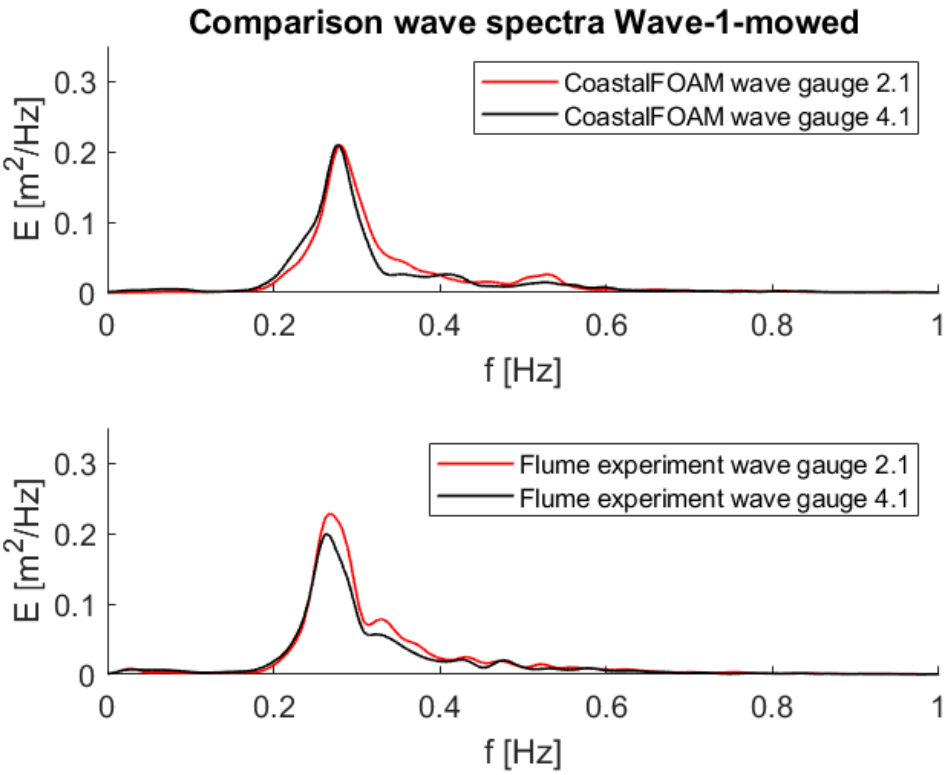

Figure 6.5: Wave-1-mowed spectra comparison: CFE vs. PFE

Figure 6.6 compares the wave spectra from the CFE with the PFE. The CFE and PFE wave spectra exhibit strong alignment.

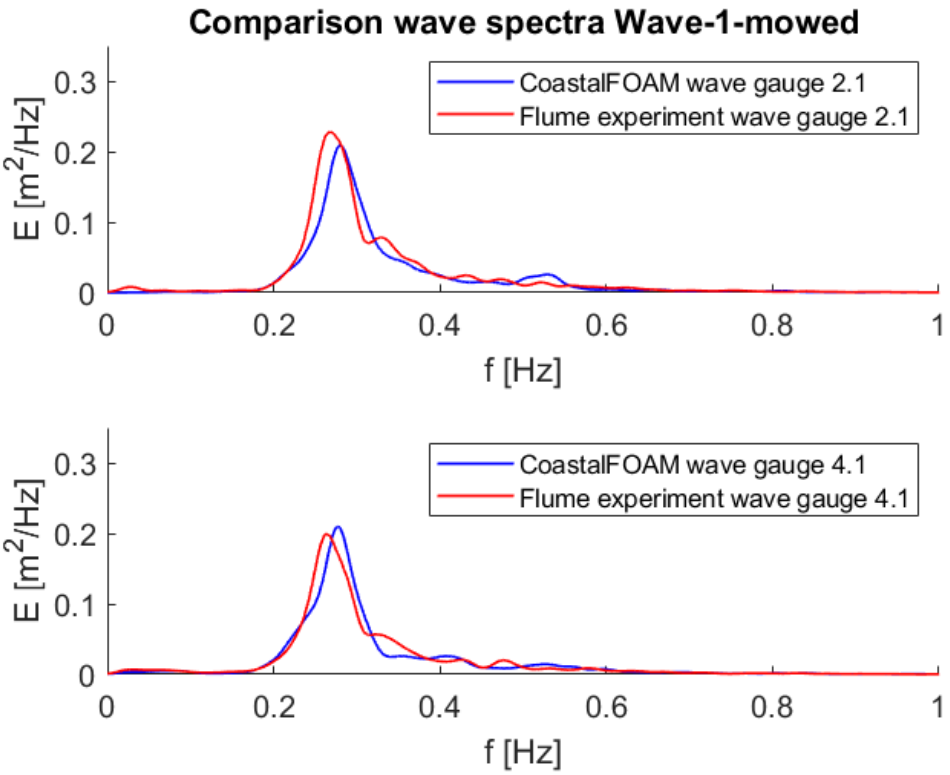

Figure 6.6: Wave-1-mowed spectra comparison: CFE vs. PFE before and after the salt marsh

7

Discussion

7.1. Relevance research

As far as is known, wave attenuation due to salt marsh vegetation has not been modelled as a porous layer in a 2D vertical CFD model before. Although the roots of mangroves have been modelled as a porous layer (Yin et al., 2023a), CFD models typically calculate wave attenuation due to vegetation using cylinders combined with a drag coefficient (Wang et al., 2020). This approach makes it not possible to calculate wave attenuation in vegetation with a 2D vertical model.

The porous layer in CoastalFOAM can now calculate wave attenuation due to salt marsh vegetation when calibrated for specific hydrodynamic conditions and salt marsh characteristics. However, this means it cannot predict wave attenuation for higher waves or changes in vegetation characteristics. Consequently, the model's current utility is limited. Nevertheless, it is promising because it accurately calculates wave attenuation and wave spectra for the base case.

The method for converting vegetation characteristics to input for the Darcy-Forchheimer equation can also be applied to other vegetation types, such as mangroves or willow forests. This is because the conversion method from salt marsh characteristics to porous layer characteristics is based on general vegetation parameters. However, the method's effectiveness must be verified as grass differs significantly from vegetation like mangroves or willow forests, for example, in terms as listed below.

- Vertical Layers: Unlike the relatively homogeneous structure of *Elymus Athericus*, mangroves and willow forests exhibit a more complex vertical layering. This layering, including roots, stems, and canopies, cannot be neglected in modelling willows and mangroves.
- Uniform Stem Distribution: Although the model assumes a densely vegetated uniform distribution of grass stems, trees often exhibit a much sparser arrangement. The gaps between trees can lead to significantly different interactions with the porous layer.
- Rigid Stems: Trees, unlike flexible grasses, are generally assumed to have rigid stems. This property better aligns with the assumption made in the section 4.2.
- Emergent Vegetation: Unlike the fully submerged grass in this study, mangroves and willow forests are normally above the water surface. The air-water interactions in the porous layer can lead to different interactions in the porous layer that represents the resistance force of the vegetation.

The differences in vertical structure, stem distribution, stem rigidity, and emergence between grasses and trees (like mangroves and willows) can have substantial consequences for the model's applicability. It is therefore crucial to explicitly address these differences when using the porous layer method to other vegetation types.

7.2. Accuracy of the model

The accuracy of the model is defined by the maximum difference in the entered value of the significant wave height and the measured significant wave height in the CoastalFOAM flume experiment after the wave development zone, as described in 5.2.2. The value of the accuracy is therefore set to 5%. This accuracy is based on the chosen mesh size and therefore it capability to mimic the hydrodynamic conditions of the physical flume experiment. This is a method with a wide margin because only percentage differences in wave reduction are actually analyzed, but the results can also be influenced by the difference in entering hydrodynamic conditions.

Other aspects besides mesh size that are influencing the model accuracy are the number of waves and the reduction of the wave height in an empty flume. The number of waves that are analyzed for the final results are 300 waves. The reason for this is because the wave spectrum does not change much anymore from 300 waves or higher. For Wave-1, comparing the significant wave height after the development zone reveals a minor difference between 0.561 meter for 300 waves and 0.556 meter for 1000 waves, representing a 0.9% difference. In practical terms, this translates to a difference of a few millimeters in wave height. The reduction in an empty flume is equal to 1.1% as already mentioned in section 5.2.2. This also goes about a reduction in significant wave height along the salt marsh vegetation of a few millimeters.

Given the relatively small significant wave heights (around 0.6 meter), precise modelling requires attention to even minor variations in significant wave height, measured in millimeters. However, when considering the scale of real-world waves and the cell size of around the water level of 0.05 meter, a few millimeters might not be practically significant. Therefore, a tolerance of 5%, which translates to a few centimeters and therefore the same order of magnitude as the cell size, could be considered as a more reasonable error margin.

7.3. KC value

The orbital velocity (u) can be measured at different points to calculate the KC number. In this research, the orbital velocity is measured at the bottom of the flume, but some sources suggest measuring it at the top of the vegetation layer (Jacobsen et al., 2017). The orbital velocity at the bottom of the vegetation layer will be lower than the maximum oscillating velocity. The KC value will therefore be lower and therefore the dampening effect will be overestimated. In short, the KC value is now determined in a way that probably overestimates the dampening effect.

Equation 7.1 is the equation used to calculate the Keulegan-Carpenter (KC) number in Moretto (2019). This equation does not require the maximum oscillating velocity. The calculated KC numbers for Wave-1, Wave-2, and Wave-1-mowed are respectively 100, 152, and 100. Comparing these values to table 5.2 confirms the consistently higher KC numbers obtained using equation 7.1 compared to the use of equation 4.7.

$$KC = \frac{H_{m0}}{2}\sqrt{\frac{g}{h}} \cdot \frac{1.1T_{m-0.1}}{D_{50}} \tag{7.1}$$

Where $T_{m-0.1}$ is the spectral wave period, which can be calculated with equation 7.2.

$$T_{m-0.1} = 0.9T_p \tag{7.2}$$

The KC value is determined in this research based on the space between the stems. According to the theory for stones D_{50} is equal to the pore size between the stones. This is different for vegetation because the stem diameter is not the same as the space between the stems. The paper of Mullarney and Henderson (2018) shows that the KC value can be determined with equation 7.3. This formula suggest that the D_{50} value should be equal to the stem diameter.

$$KC = uT/S_d \tag{7.3}$$

When the use of S_d instead of D_{50} is also included in the calculation of KC using equation 7.4, the resulting values for Wave-1, Wave-2, and Wave-1-mowed are 177, 268, and 177, respectively. By examining the effect of these KC values on beta in equation 5.1, the maximum impact on beta is 5.7%. For Wave-2, a 16.7% reduction in β leads to a 3.6% decrease in wave height. Consequently, the overall results will be influenced by about 1%. However, since β is a calibrated parameter with the KC value already taken into account, the research itself and the differences in hydrodynamic conditions before and after vegetation are not significantly affected. While the impact on damping for this study is minimal, it is still advisable to reconsider the calculation of KC and to employ the equations discussed in this section.

$$KC = \frac{H_{m0}}{2}\sqrt{\frac{g}{h}} \cdot \frac{1.1T_{m-0.1}}{S_d} \tag{7.4}$$

7.4. Higher wave (Wave-2)

The dampening effect of the porous layer, as seen in section 6.2, is overestimated also with the relationship made between the drag coefficient and the β value. The same vegetation characteristics as in wave-1 were used. The only differences are the hydrodynamic conditions. Apparently, this does not lead to the correct results. Section 4.4 discusses that the effect of the KC number will result in less dampening for higher values of the peak wave period and the significant wave height. Apparently this reduction due to the higher KC number does not result in the results of the PFE.

Equation 5.1 is primarily fixed, with the calibration constant β as the only adjustable parameter. The paper of Möller et al. (2014) observed that higher waves naturally increase orbital velocity, leading to greater plant bending. Consequently, the current β value, even when adjusted with C_d, overestimated the wave attenuation for higher waves. A potential solution involves establishing a relationship between β and plant bending through calibration for the porous layer. Additionally, the difference between PFE and CFE wave spectra observed in section 6.2 could contribute to this wrong predicted wave attenuation. Reflection analyses indicate no significant increase in the reflective wave relative to Wave-1.

7.5. Lower vegetation height (Wave-1-mowed)

The damping observed in section 6.3 appears to be underestimated. The reason for the underestimation of the wave height reduction could be that bottom friction was not initially accounted for in the model. Although the effect of bottom friction was incorporated into the porous layer by the calibration for Wave-1, this effect could diminishes with lower vegetation height. The reason for this is because the bottom friction could become more important because the vegetation height reduces. Consequently, the method of modeling bottom friction may be incorrect. It may not be feasible to combine these two factors into a single porous layer, or it may not be possible to adjust the vegetation height effectively.

Based on the assumptions in section 4.2, the assumption of rigid stems could be contributing to the observed underestimation of wave damping. Plant bending may be underestimated in the current model, as the porous layer calibration assumed non-bending plants. With longer stems the grass bends more easily due to increased momentum. Therefore, the shorter grass in Wave-1-mowed may be experiencing less bending, leading to an underestimation of its resistance force. Consequently, this could result in an underestimation of wave damping, which aligns with the findings. The calibration parameter β should therefore be increased in equation 5.1.

The reason of the underestimation for Wave-1-mowed could therefore be due to the incorporation of bottom friction in the porous layer or the assumption of rigid stems for the Wave-1 case.

8

Conclusion

The main research question, ‘How can a porous layer within CoastalFOAM be used to model wave attenuation during storm conditions by salt marsh vegetation at the foreshore of a dike?’, will be answered in this chapter by answering the sub-questions from chapter 1.

1. What experimental conditions and wave attenuation measurements are needed to calibrate the CoastalFOAM model for simulating wave attenuation by salt marsh vegetation?
The experimental conditions required to study wave attenuation by a salt marsh can be categorized into two main aspects: hydrodynamic conditions and vegetation characteristics. The hydrodynamic conditions include the significant wave height (H_{m0}), water depth (z), and peak wave period (T_p). These conditions are used to characterize irregular waves. It is essential to know these hydrodynamic parameters both before and after the vegetation zone. In terms of vegetation characteristics, the parameters of interest are stem diameter (S_d), stem height (S_h), stem density (S_n), and the length of the salt marsh.

The selected case study for this research is part of ‘Project Bassia’ and involves a flume experiment described in the paper by Möller et al. (2014). The flume experiment is focused on the wave attenuation properties of a salt marsh dominated by the species *Elymus athericus*. Measurements of water surface elevation were taken upstream and downstream of the vegetation to assess the impact on wave properties.

A specific scenario from ”Project Bassia” study has been chosen as the base case for model calibration. Additional tests were conducted to observe the effects of variations in both hydrodynamic and vegetation characteristics. For the hydrodynamic conditions, alterations included an increase in significant wave height (H_{m0}) and a longer peak wave period (T_p). Regarding vegetation characteristics, a scenario with reduced stem height (S_h) was selected.

The base case shows a wave attenuation of 18.1%. The test with a higher wave and higher wave period shows a attenuation rate of 13.9%, and the test with lower vegetation height resulted in a lower attenuation of 7.5%. Notably, the presence of the salt marsh increased wave attenuation, as evidenced by the difference in vegetation height. The wave spectra predominantly showed a reduction in wave energy at higher frequencies.

2. How to apply the method to calculate porous media flow through a stone layer to simulate the wave attenuation by a salt marsh?
The method is designed to calculate the flow velocity reduction for a stone layer but needs to be adapted to determine the wave attenuation for a salt marsh. In the model, the stone layer is represented as a

porous layer. The damping effect of the porous layer is calculated using the Darcy-Forchheimer equation. For a stone layer, the physical characteristics are defined by the median grain size (D_{50}) and porosity (n_p). In the case of a salt marsh, the vegetation is modeled as rigid cylindrical stems that are uniformly distributed.

The median grain size (D_{50}) represents the pore size of the porous layer, therefore the median grain size is equated to the distance between the stems of the grass. The porosity (n_p) is considered as the ratio between the total volume from the ground to the stem height and the same volume excluding the stems themselves. Although the physical parameters can now be determined, the Darcy-Forchheimer equation includes three additional calibration parameters: α, β, and KC. The values of α and β determine the relative importance of laminar and turbulent flow within the equation. This importance is assessed using the porous Reynolds number (Re_p).

The value of (Re_p) is higher than 300, which indicates that α, representing the damping of laminar flow, is negligible, leaving only β, representing the damping of turbulent flow, to be calibrated. As a result, the focus shifts to the Forchheimer equation. Various studies have established a correlation between vegetation damping and KC, which is why it is included in the calculation of the damping effect. The calculation of the KC number needs reconsideration as mentioned in section 7.3. With all parameters of the Darcy-Forchheimer equation known, the calibration of β remains. To determine the true value, a range of values between 2 and 5 is explored to interpolate the precise value of β. After calibration of the base case, a value of 4.84 is found for β.

3. What differences exist in the calculated wave attenuation between the physical flume experiment and the CoastalFOAM flume experiment?
The selected mesh size directly impacts model accuracy, which is primarily assessed by the model's ability to accurately replicate the significant wave height of the PFE in the CFE after the wave development zone. As explained in section 7.2, this approach is more reasonable than evaluating accuracy based on wave height reduction along the flume or the number of waves, as these metrics involve changes in millimeters, which might appear insignificant in the context of real-world waves and the chosen mesh size of 0.05 meter.

In the Wave-1 case, which is the case that the model is calibrated on, the resulting simulation showed a 18.4% wave height attenuation, whereas it should be 18.1%. This value lies within the accuracy interval. The wave spectra and the peak wave period in the CFE align with the results of the PFE.

The Wave-2 scenario with higher waves shows that the observed wave reduction was 13.9%, which is significantly lower than the modelled reduction of 23.6%. This difference indicates that the damping effect of the porous layer is overestimated. Consequently, the β value is adjusted according the percentile change in C_d in the study of Möller et al. (2014). The CFE now shows a reduction in wave height of 20%, which still overestimates the damping. A potential solution involves establishing a relationship between β and plant bending through calibration for the porous layer. Additionally, the difference between PFE and CFE wave spectra observed in section 6.2 could contribute to this wrong predicted wave attenuation.

The Wave-1-mowed test, featuring lower vegetation, observed a 7.5% wave reduction, while the CFE indicated only a 2.5% reduction, highlighting a significant underestimation. This difference may be attributed to the incorporation of bottom friction within the porous layer or the assumption of rigid stems. Addressing bottom friction could involve separate modeling of the porous layer and bottom friction. To address the rigid stem assumption, a relationship between β and reduced vegetation height must be established to account for the increased resistance force resulting from decreased plant bending.

9

Recommendations

9.1. Separating bottom friction from the porous layer

Section 7.5 demonstrated that the underestimation of the damping effect for the lower vegetation height is possibly due to the incorporation of bottom friction within the porous layer. To address this, it is recommended to separate the bottom friction from the porous layer for the vegetation. Two approaches to achieve this are outlined below:

- The first approach is to separate the bottom friction from the porous layer by applying a gradient boundary condition at the bottom.
- The second approach involves using two separate porous layers. The bottom layer should be calibrated for the mowed condition accounting for both the bottom friction and the vegetation layer close to the ground. The mowed vegetation layer will exhibit lower bending angles, and therefore does not be influenced by the effect of losing damping capacity by higher waves as described in section 7.4. The layer above the mowed vegetation height can then be calibrated using a bending relationship for β, as described in section 9.2.

9.2. Relationship calibration parameter and plant bending

Section 7.4 demonstrated that the overestimation of the dampening effect for higher waves is possibly due to the increased bending of the stems under such hydrodynamic conditions as in Wave-2. Section 7.5 shows that the underestimation of damping effect for lower vegetation height is possibly due to the decreased bending angle of the stems for such vegetation characteristics as in Wave-1-mowed. To address this, it is recommended to incorporate a relationship between the change in hydrodynamic conditions or the vegetation characteristics and the bending angle of the plant into the β value. This approach would eliminate the need for constant model calibration and allow to make predictions of changes in hydrodynamic conditions or vegetation characteristics beyond those physically tested. While the study of Möller et al. (2014) established a relationship between hydrodynamic conditions, plant bending, and drag coefficient (Cd), this relationship can not be directly applied to the porous layer approach. Section 5.3 also showed that the same resistance force between equation 2.4 and equation 5.1 does not produce the same wave height reduction. A new relationship for the porous layer and a change in hydrodynamic conditions and vegetation characteristics will then have to be established by calibration.

9.3. Mangroves and willow forests

The adaptation of the porous layer characteristics is based on general vegetation characteristics. This method can also be applied to mangroves or willow forests. It is hereby important to consider the assumptions associated with modeling trees as a porous layer, as discussed in section 7.1. It would be interesting to see if the CoastalFOAM model, combined with the porous layer approach, can accurately calculate wave attenuation by mangroves or willow forests.

References

Adesina, R. B., He, Z., Oladejo, H. O., Dada, O. A., & Ajibade, H. J. (2024). High-resolution wave modeling of the Southwestern Nigerian coastal shelf: Implications on geomorphic contrasts between barrier-lagoon and mud coasts. *Marine Geology*, *470*. https://doi.org/10.1016/j.margeo.2024.107253

Boersen, S., Scholl, O., Jacobsen, N., Van Der Lem, C., & HaskoningDHV, R. (2019). *APPLYING A NUMERICAL WAVE FLUME TO PREDICT WAVE OVERTOPPING* (tech. rep.). https://doi.org/10.3850/38WC092019-1337

Bouma, T. J., van Belzen, J., Balke, T., Zhu, Z., Airoldi, L., Blight, A. J., Davies, A. J., Galvan, C., Hawkins, S. J., Hoggart, S. P., Lara, J. L., Losada, I. J., Maza, M., Ondiviela, B., Skov, M. W., Strain, E. M., Thompson, R. C., Yang, S., Zanuttigh, B., … Herman, P. M. (2014). Identifying knowledge gaps hampering application of intertidal habitats in coastal protection: Opportunities & steps to take. *Coastal Engineering*, *87*, 147–157. https://doi.org/10.1016/j.coastaleng.2013.11.014

Brooks, H., Moeller, I., Spencer, T., & Royse, K. (2023). Shear strength and erosion resistance of salt marsh substrates: Which method to use? *Estuarine, Coastal and Shelf Science*, *292*. https://doi.org/10.1016/j.ecss.2023.108452

Çete, C. (2019). *Quantifying the effect of woody vegetation on the wave loads on a dike using remote sensing Large scale physical model tests* (tech. rep.). http://repository.tudelft.nl/.

De Jesus Crespo, R., Wu, J., Myer, M., Yee, S., & Fulford, R. (2019). Flood protection ecosystem services in the coast of Puerto Rico: Associations between extreme weather, flood hazard mitigation and gastrointestinal illness. *Science of the Total Environment*, *676*, 343–355. https://doi.org/10.1016/j.scitotenv.2019.04.287

Dronkers, J. (2020). Coastalwiki. https://www.coastalwiki.org/wiki/File:RearSideFailure.jpg

Esselink, P., van Duin, W., Bunje, J., Cremer, J., Folmer, E., Frikke, J., Glahn, M., de Groot, A., Hecker, N., Hellwig, U., Jensen, K., Körber, P., Petersen, J., Stock, M., & Groot, d. A. (2017). *Wadden Sea Quality Status Report Salt marshes Wadden Sea Quality Status Report-Salt marshes 2 Colophon* (tech. rep.).

Ghasemi, A., Amirabadi, R., Kamalian, U. R., & Mazyak, A. R. (2023). Numerical modeling investigation of perforated geometry of caisson breakwater under irregular waves by considering porous media. *Ocean Engineering*, *269*. https://doi.org/10.1016/j.oceaneng.2022.113558

Haddad, J., Rosman, J. H., Luettich, R. A., & Voss, C. M. (2024). Canopy drag parameterization from field observations for modeling wave transformation across salt marshes. *Coastal Engineering*, *187*. https://doi.org/10.1016/j.coastaleng.2023.104407

He, Y., Chen, H., Yang, H., He, D., & Dong, G. (2023). Experimental investigation on the hydrodynamic characteristics of extreme wave groups over unidirectional sloping bathymetry. *Ocean Engineering*, *282*. https://doi.org/10.1016/j.oceaneng.2023.114982

Horstman, E. M., Dohmen-Janssen, C. M., Narra, P. M., van den Berg, N. J., Siemerink, M., & Hulscher, S. J. (2014). Wave attenuation in mangroves: A quantitative approach to field observations. *Coastal Engineering*, *94*, 47–62. https://doi.org/10.1016/j.coastaleng.2014.08.005

Horstman, M. C. (2020). *Feasibility assessment of a grass cover dike in a coastal wetland setting Towards a design tool* (tech. rep.).

Hughes, R. G. (2004). Climate change and loss of saltmarshes: Consequences for birds. *Ibis*, *146*(SUPPL.1), 21–28. https://doi.org/10.1111/j.1474-919X.2004.00324.x

Jacobsen, N. G., van Gent, M. R., Capel, A., & Borsboom, M. (2018). Numerical prediction of integrated wave loads on crest walls on top of rubble mound structures. *Coastal Engineering*. https://doi.org/10.1016/j.coastaleng.2018.10.004

Jacobsen, N. G., van Gent, M. R., & Fredsøe, J. (2017). Numerical modelling of the erosion and deposition of sand inside a filter layer. *Coastal Engineering*. https://doi.org/10.1016/j.coastaleng.2016.09.003

Jensen, B., Jacobsen, N. G., & Christensen, E. D. (2014). Investigations on the porous media equations and resistance coefficients for coastal structures. *Coastal Engineering*, *84*, 56–72. https://doi.org/10.1016/j.coastaleng.2013.11.004

Karola, A., Tavakoli, S., Mikkola, T., Matusiak, J., & Hirdaris, S. (2024). The influence of wave modelling on the motions of floating bodies. *Ocean Engineering*, *306*. https://doi.org/10.1016/j.oceaneng.2024.118067

Lambers, M. (2022). *How vegetated foreshores can contribute to limiting dike dimensions of sea dikes A case study into the assessment and design procedure of including the quantitative effect of the foreshore in the flood defence system* (tech. rep.). https://www.magazinesrijkswaterstaat.nl/mer-nieuws/2020/94/brede-groene-dijk

Liu, S., Xu, S., & Yin, K. (2023). Optimization of the drag coefficient in wave attenuation by submerged rigid and flexible vegetation based on experimental and numerical studies. *Ocean Engineering*, *285*. https://doi.org/10.1016/j.oceaneng.2023.115382

Maza, M., Lara, J. L., & Losada, I. J. (2016). Solitary wave attenuation by vegetation patches. *Advances in Water Resources*, *98*, 159–172. https://doi.org/10.1016/j.advwatres.2016.10.021

Maza, M., Lara, J. L., & Losada, I. J. (2015). Tsunami wave interaction with mangrove forests: A 3-D numerical approach. *Coastal Engineering*, *98*, 33–54. https://doi.org/10.1016/j.coastaleng.2015.01.002

Mendez, F. J., & Losada, I. J. (2004). An empirical model to estimate the propagation of random breaking and nonbreaking waves over vegetation fields. *Coastal Engineering*, *51*(2), 103–118. https://doi.org/10.1016/j.coastaleng.2003.11.003

Möller, I., Kudella, M., Rupprecht, F., Spencer, T., Paul, M., Van Wesenbeeck, B. K., Wolters, G., Jensen, K., Bouma, T. J., Miranda-Lange, M., & Schimmels, S. (2014). Wave attenuation over coastal salt marshes under storm surge conditions. *Nature Geoscience*, *7*(10), 727–731. https://doi.org/10.1038/NGEO2251

Moretto, M. L. A. (2019). *An efficient numerical approach to model wave overtopping of rubble mound breakwaters* (tech. rep.). http://repository.tudelft.nl/.

Mullarney, J. C., & Henderson, S. M. (2018). *Chapter 1 Flows Within Marine Vegetation Canopies* (tech. rep.). www.worldscientific.com

O'hara, B. (2017). Blue Carbon Runs Deep: An Assessment of Sediment Carbon Stocks in Delaware Bay Salt Marshes. https://doi.org/10.13140/RG.2.2.11694.61765

OpenCFD. (2019). OpenFOAM:User Guide v2112. https://www.openfoam.com/documentation/guides/latest/doc/index.html

Paul, M., Rupprecht, F., Möller, I., Bouma, T. J., Spencer, T., Kudella, M., Wolters, G., van Wesenbeeck, B. K., Jensen, K., Miranda-Lange, M., & Schimmels, S. (2016). Plant stiffness and biomass as drivers for drag forces under extreme wave loading: A flume study on mimics. *Coastal Engineering*, *117*, 70–78. https://doi.org/10.1016/j.coastaleng.2016.07.004

Paulsen, B. T., Bredmose, H., & Bingham, H. B. (2014). An efficient domain decomposition strategy for wave loads on surface piercing circular cylinders. *Coastal Engineering*, *86*, 57–76. https://doi.org/10.1016/j.coastaleng.2014.01.006

Phan, K. L., Stive, M. J., Zijlema, M., Truong, H. S., & Aarninkhof, S. G. (2019). The effects of wave non-linearity on wave attenuation by vegetation. *Coastal Engineering*. https://doi.org/10.1016/j.coastaleng.2019.01.004

Rupprecht, F. (2015). *Vegetation succession and coastal protection by wave dissipation in salt marshes of North-West Europe* (tech. rep.).

Schiereck, G. J., & Verhagen, H. J. (2012). *Introduction to bed, bank and shore protection* (tech. rep.).

Stark, J., Plancke, Y., Ides, S., Meire, P., & Temmerman, S. (2016). Coastal flood protection by a combined nature-based and engineering approach: Modeling the effects of marsh geometry and surrounding dikes. *Estuarine, Coastal and Shelf Science*. https://doi.org/10.1016/j.ecss.2016.03.027

Takagi, H. (2023). Survival of young planted mangroves in a calm bay environment during a tropical cyclone. *Nature-Based Solutions*, *4*, 100082. https://doi.org/10.1016/j.nbsj.2023.100082

The Open University. (1999). Waves, Tides and Shallow-Water Processes.

van der Werf, J. J. (2022). *Wave-Dominated Coastal Dynamics-Lecture Notes* (tech. rep.).

van Heest, M. F. (2022). *Numerical estimation of upward pressure differences over a placed block revetment under wave loading on a dike* (tech. rep.).

van Koelen, L. P. (2022). *Using CFD to design riprap bed protections downstream of underflow weirs Weir design of the future* (tech. rep.). http://repository.tudelft.nl

van Veelen, T. J., Fairchild, T. P., Reeve, D. E., & Karunarathna, H. (2020). Experimental study on vegetation flexibility as control parameter for wave damping and velocity structure. *Coastal Engineering*, *157*. https://doi.org/10.1016/j.coastaleng.2020.103648

van Wesenbeeck, B. K., Wolters, G., Antolínez, J. A., Kalloe, S. A., Hofland, B., de Boer, W. P., Çete, C., & Bouma, T. J. (2022). Wave attenuation through forests under extreme conditions. *Scientific Reports*, *12*(1). https://doi.org/10.1038/s41598-022-05753-3

Vázquez-Lule, A., & Vargas, R. (2021). Biophysical drivers of net ecosystem and methane exchange across phenological phases in a tidal salt marsh. *Agricultural and Forest Meteorology*, *300*. https://doi.org/10.1016/j.agrformet.2020.108309

Vuik, V., Jonkman, S. N., Borsje, B. W., & Suzuki, T. (2016a). Nature-based flood protection: The efficiency of vegetated foreshores for reducing wave loads on coastal dikes. *Coastal Engineering*, ((a)). https://doi.org/10.1016/j.coastaleng.2016.06.001

Vuik, V., Van Vuren, S., & Jonkman, S. N. (2016b). Nature-based flood protection: Using vegetated foreshores for reducing coastal risk. *E3S Web of Conferences*, *7*. https://doi.org/10.1051/e3sconf/20160713014

Wang, Y., Yin, Z., & Liu, Y. (2020). Numerical investigation of solitary wave attenuation and resistance induced by rigid vegetation based on a 3-D RANS model. *Advances in Water Resources*, *146*. https://doi.org/10.1016/j.advwatres.2020.103755

Willemsen, P. W., Borsje, B. W., Vuik, V., Bouma, T. J., & Hulscher, S. J. (2020). Field-based decadal wave attenuating capacity of combined tidal flats and salt marshes. *Coastal Engineering*, *156*. https://doi.org/10.1016/j.coastaleng.2019.103628

Yin, K., Lin, M., Xu, S., Hao, J., Mao, L., & Li, M. (2023b). Numerical investigation of submerged flexible vegetation dynamics and wave attenuation under combined waves and following currents. *Ocean Engineering*, *278*. https://doi.org/10.1016/j.oceaneng.2023.114437

Yin, Z., Li, J., Wang, Y., Wang, H., & Yin, T. (2023a). Solitary wave attenuation characteristics of mangroves and multi-parameter prediction model. *Ocean Engineering*, *285*. https://doi.org/10.1016/j.oceaneng.2023.115372

Zhu, L., Chen, Q., Ding, Y., Jafari, N., Wang, H., & Johnson, B. D. (2023). Towards a unified drag coefficient formula for quantifying wave energy reduction by salt marshes. *Coastal Engineering*, *180*. https://doi.org/10.1016/j.coastaleng.2022.104256

A

Project Bassia

In addition to section 3.1, this appendix gives some extra information about Project Bassia. Project Bassia (biodiversity, management and ecosystem functions of Salt marshes in the Wadden Sea National Park of Schleswig-Holstein) is an umbrella name for the project (Rupprecht, 2015). The interest for this research lies in the flume experiment, which was conducted in the large wave flume (Grosser Wellenkanal, GWK) of Forschungzentrum Küste (FZK) in Hannover, Germany. The flume experiment tests the wave attenuation by a salt marsh (Möller et al., 2014).

The case studies that are selected from the tests from (Möller et al., 2014) are highlighted in table A.1. 'Wave 1', 'wave 2', and 'wave 1 mowed' are respectively test date and number: 20131021_6, 20131022_4, and 20131031_9. The case 20121031_11 was not selected because a few individual waves in that series broke.

Table A.1: Complete overview of wave tests (Möller et al., 2014)

Test date & Number	Vegetated or Mowed	T_p	$H_{rms,0}$ Front	$H_{rms,0}$ Back
20131015_1	Vegetation	1,5	0,118	0,11
20131015_3	Vegetation	2,1	0,204	0,18
20131015_5	Vegetation	2,9	0,198	0,17
20131017_1	Vegetation	2,9	0,197	0,17
20131017_4	Vegetation	2,5	0,287	0,25
20131017_6	Vegetation	3,6	0,296	0,24
20131021_1	Vegetation	2,9	0,378	0,32
20131021_4	Vegetation	4,1	0,398	0,33
20131021_6	**Vegetation**	**3,6**	**0,571**	**0,47**
20131022_4	**Vegetation**	**5,1**	**0,602**	**0,51**
20131024_1	Vegetation	4,1	0,740	0,63
20131024_3	Vegetation	5,8	0,780	0,66
20131024_6	Vegetation	4,4	0,830	0,70
20131025_1	Vegetation	6,2	0,870	0,72
20131029_1	Mowed	2,9	0,377	0,35
20131029_4	Mowed	4,1	0,400	0,37
20131031_9	**Mowed**	**3,6**	**0,573**	**0,52**
20131031_11	Mowed	4,1	0,741	0,67

The vegetation characteristics of the salt marsh are known and shown in table A.2. The vegetation in the flume exist of three types of vegetation *Puccinellia maritima*, *Elymus athericus*, and *Atriplex prostrata*. *Elymus athericus* is the dominant vegetation type and in the paper of (Möller et al., 2014),

the calculation of the vegetation drag coefficient is only based on the characteristics of this vegetation type. The same assumption will be made for this research and therefore the drag force due to the other vegetation types will be neglected.

Table A.2: Vegetation characteristics of 'Project Bassia'

	S_h (mm)	S_d (mm)	S_n (number per 20 x 20 cm quadrat)
Puccinellia maritima	220 +- 30	1.1 +- 0.3	Unknown
Elymus athericus	700 +- 10	1.3 +- 0.3	68 +- 8
Atriplex prostrata	Unknown	Unknown	Unknown

The timeseries of the water surface elevation are analysed and the range of time that is analysed in the timeseries is shown in table A.3.

Table A.3: Time range of the analysed timeseries for PFE

Test name	range of time [s]
Wave-1	100-3700
Wave-2	100-5000
Wave-1-mowed	100-3700

B

Project Be Safe

In addition to section 3.1, this appendix gives some extra information about Project BE SAFE. Project BE SAFE is a research program in The Netherlands about bio-Engineering for safety using vegetated foreshores. For this research the interest goes to a field experiment. The wave attenuation by salt marshes is measured in Hellegat and Bath, both located in the province of Zeeland. (Vuik et al., 2016a). This overview of this field experiment shows an alternative case study.

Figure B.1 provides an overview of the field experiment. The wave height (H_{m0}) varies between 0.07 and 0.69 meter, and the water level ranges from 0.32 to 2.52 meter. The water depth along the salt marsh also varies due to the uneven bathymetry and a slope of 1:100. Wave height measurements are taken at four positions: before and after the vegetation, and at the beginning and within the salt marsh. The vegetation height is approximately 0.30 meter. The salt marsh consists of two types of grasses: cordgrass (*Spartina anglica*) and grassweed (*Scirpus maritimus*). The characteristics of these grasses are shown in table B.1.

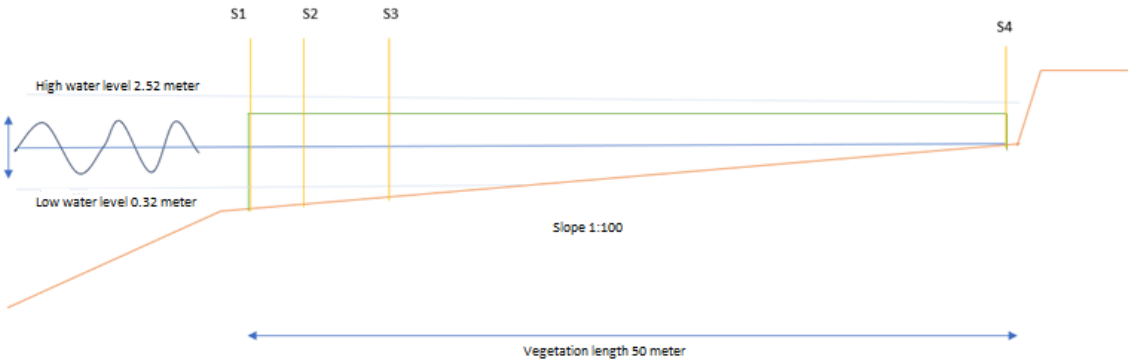

Figure B.1: Overview of field experiment 'Project BESAFE'

Table B.1: Vegetation characteristics 'Project BESAFE'

Sample	S_h $[m]$	S_n $[stems/m^2]$	S_d $[m]$
Hellegat S1-S2	0.20	944	0.003
Hellegat S2-S3	0.29	1136	0.0034
Hellegat S3-S4	0.27	1520	0.0027
Bath S1-S2	0.17	144	0.0087
Bath S2-S3	0.15	372	0.008
Bath S3-S4	0.35	1072	0.0049

C

CoastalFOAM mesh

In addition to section 5.2.2, this appendix gives some extra information about the reduction of the wave height due to different mesh sizes. For all these block mesh sizes, a refinement around the water level was applied. A different geometry and location of the wave gauges shown in figure C.2 was used compared to figure 2.8, because the exact location of the wave gauges were not yet known at the time the mesh size was determined.

Figure C.1 illustrates a correlation between increased mesh size and wave reduction in an empty numerical flume. This increase is attributed to an increase in numerical dispersion due to the larger mesh size. To maintain acceptable accuracy, this numerical dispersion must remain below 5%. Additionally, minor variations in determining significant wave height along the flume are visible influenced by the wave gauge's location.

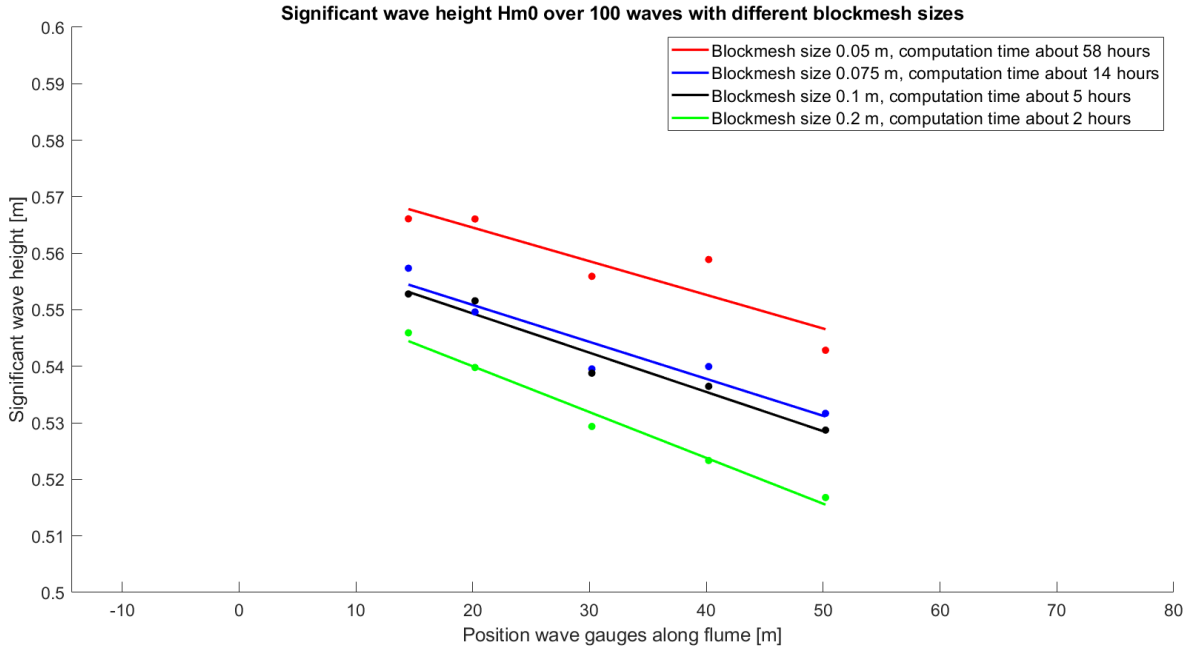

Figure C.1: Reduction in significant wave height between first and second wave gauge set for different cell sizes

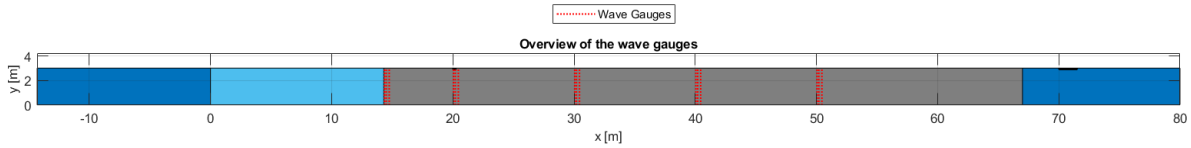

Figure C.2: Numerical wave flume related to the reduction test in significant wave height for different cell sizes

D

CoastalFOAM general settings

CoastalFOAM is a numerical wave flume model built in OpenFOAM. OpenFOAM works with a folder structure and runs on Linux. A basic version of this folder structure is explained, as well as essential parts of the creation of the model. The elaborated version of how OpenFOAM works can be found in the manual OpenCFD (2019). Finally, the time range used to analyse the water surface elevation time series are given for the different tests.

Folder structure

OpenFOAM operates within a structured folder system. Within the case folder there are three primary folders: 0, constant, and system.

- The '0' folder contains the initial and boundary conditions for each variable that is modelled.
- In the 'constant' folder the information regarding the mesh, model constants, wave properties, and wave porous layer characteristics are stored.
- The 'system' folder controls the simulation, including files on the solution procedure, additional meshing procedures, time step definitions and parallel computations.

Applied OpenFOAM commands

In this subsection the applied comands for the model runs are summarised. The commands are provided in chronological order and contain a short explanation to understand what the command does (van Koelen, 2022).

- BlockMesh - The basis geometry and mesh is created.
- FaceSetToSTL - This command makes it possible to create various shapes, which can later on be cut out of the Blockmesh.
- SnappyHexmesh - This command makes it possible to add refinements, such as the refinement around the water level.
- Extrudemesh - This command prepares your grid for a 2D simulation by redefining the SnappyHesmesh surfaces.
- Checkmesh - This command checks your mesh on skewness and other mesh parameters.
- DecomposePar - This command decomposes the mesh into multiple pieces, allowing parallel running on different processors.
- Mpirun - Run command for the decomposed mesh. After this command, the simulation is actually calculating and not preparing the calculation anymore.
- ReconstructPar - Reconstructs the decomposed files into one file in the main directory.

Range of time for performed tests

The timeseries of the water surface elevation for the CoastalFOAM experiment are analysed and the range of time that is analysed in the timeseries is shown in table D.1.

Table D.1: Time range of the analysed timeseries for CFE

Test name	Range of time [s]
Wave-1	20-3620
Wave-2	30-4930
Wave-1-mowed	20-3620